NTNU – Trondheim
Norwegian University of
Science and Technology

Cosmic Rays from Pair-Instability Supernova Remnants

Marie Kristine Foss

MSc in Physics
Submission date: May 2015
Supervisor: Michael Kachelriess, IFY

Norwegian University of Science and Technology
Department of Physics

Abstract

Pair-instability supernovae are the most energetic thermonuclear explosions in the Universe, up to 100 times more energetic than type Ia supernovae. Around redshift $z \gtrsim 6$ approximately one out of ten supernovae was a pair-instability supernova. In the local universe, however, this number is drastically reduced to less than one out of ten thousand. In this thesis we look at progenitors both among the first generation of stars and in the local universe. We determine the dynamical evolution of the supernova blast wave propagating through the interstellar medium. The maximum energy a cosmic ray proton can be accelerated to in the supernova remnant is then found to be $4 \times 10^{15}\,\mathrm{eV}$, for a mean magnetic field of $100\,\mu\mathrm{G}$ parallel to the shock front. Lastly, the proton and neutrino flux for a Pop III pair-instability supernova is estimated. The diffuse neutrino flux for Pop III PI SNe is found to be a sub-dominant contribution to the observed flux.

Sammendrag

Par-ustabile supernovaer er de mest energifulle eksplosjonene i universet, og frigir opp til 100 ganger mer energi enn type Ia supernovaer. Tidlig i universets historie (rødforskyvning $z \gtrsim 6$) var en av ti supernovaer en par-ustabil supernova. I det lokale universet er dette tallet drastisk redusert til mindre enn en av ti tusen. I denne masteroppgaven ser vi på forgjengere både blant den første generasjonen av stjerner og stjerner i det lokale universet. Vi bestemmer først hvordan en eksplosjonsbølge som følge av en par-ustabil supernova beveger seg gjennom det interstellare medium. Den høyeste energien proton kan akselereres opp til i en supernovarest ble funnet til å være $4 \times 10^{15}\,\mathrm{eV}$ når magnetfeltet i supernovaresten ble satt til å være gjennomsnittlig $100\,\mu\mathrm{G}$. Til sist estimeres fluksen av protoner og nøytrinoer fra alle par-ustabile supernovaer for $z \gtrsim 6$. Den isotropiske fluksen av nøytrinoer viste seg å bidra svært lite til den målte bakgrunnen av nøytrinoer.

Acknowledgement

I would like to thank my supervisor, Professor Michael Kachelriess, for all the advise and guidance. My family and friends back home for keeping me motivated, and proofreading, even though they did not understand a thing. And lastly, all the other students assigned to room B3-103 for studying mostly at home, providing me with the quiet work atmosphere I prefer.

Contents

List of Figures

List of Tables

Abbreviations

MS	=	Main Sequence
HR	=	Hertzsprung-Russel
SN	=	Supernova
PI	=	Pair-Instability
PPI	=	Pulsational Pair-Instability
CC	=	Core Collapse
ISM	=	Interstellar Medium
EoS	=	Equation of State
SNR	=	Supernova Remnant
ED	=	Ejecta Dominated
ST	=	Sedov-Taylor
PDS	=	Pressure-Driven Snowplow
SFR	=	Star Formation Rate

Introduction

Pair-instability supernovae are the most energetic thermonuclear explosions in the Universe. The ejected energy is typically around 10^{52} erg, with the most massive ones being almost 100 times more energetic than a type Ia supernova. After carbon burning, the temperature in the core of the progenitor is so high that electron and positron pairs are created, which causes an instability, hence the name. The core contracts until oxygen and silicon ignites explosively, and the star is completely blown apart, leaving no remnant core.

Pair-instability supernovae are believed to have been very common for the first generation of stars, and central for the chemical enrichment of the Universe. The first stars (Population III or just Pop III) are assumed to have been very massive and metal-free. Pop III stars more massive than $65\,M_\odot$ can encounter pair-instability, but have to be within the range of $(150 - 260)\,M_\odot$, or $(90 - 140)\,M_\odot$ if they are rotating, to die as a pair-instability supernova. During the supernova explosion, huge amounts of ^{56}Ni are released, and heavier elements are created.
As it turns out pair-instability in the core is not exclusive to Pop III stars, as there are some firm pair-instability supernova candidates in the local universe. It is not understood how such massive stars can form in high metallicity environments. One possibility is the merging of stars in young, dense clouds. Either way, massive ($M > 150\,M_\odot$) stars have been observed in the local universe.

This thesis starts with some background information about stellar evolution in chapters 1 and 2. In chapter 3 we take a closer look at pair-instability supernovae. We discuss fluid dynamics in chapter 4, a topic needed to understand the supernova shock. In chapter 5 we look at the analytic solution to the dynamical evolution of the blast wave into the interstellar medium. And finally a consequence of the explosion, acceleration of cosmic rays in chapter 6. Here we discuss diffusive particle acceleration and how to calculate the maximum energy of a cosmic ray and the cosmic ray flux. Along the way, theory is used to find some properties pair-instability supernovae with both local and Population III progenitors. Finally, in chapter 7, we sum up the thesis and look at what is to come.

Chapter 1

The Evolution of Stars

A star is a body that is bound by self-gravity and that radiates energy supplied by an internal source. There are three main stages of stellar evolution; the formation, the main-sequence (MS) phase, and the most interesting one, the post-main-sequence phase. For a more detailed picture see [8] or [9]. All stars can be organized in a Hertzsprung-Russell (HR) diagram, by surface temperature and luminosity. An example is given in figure 1.1. The thick, diagonal line are all stars in the MS phase, the extension to the upper right are red giants, and the ones on the lower left are white dwarfs.

1.1 Star Formation

Stars are born in giant gaseous, low-density clouds. These clouds are often subject to perturbations which lead to a region of higher density, increased gas pressure and increased gravitational pull. If the cloud is unstable, it can collapse and form stars. Consider a uniform, spherical cloud with mass M, radius R, and temperature T. The gravitational energy is then

$$V = -\frac{3}{5}\frac{GM^2}{R}, \tag{1.1}$$

where G is the gravitational constant, and the kinetic energy is

$$K = \frac{3}{2}\frac{M}{m}k_{\mathrm{B}}T. \tag{1.2}$$

Here, m is the mass per particle and k_{B} the Boltzmann constant. For the cloud to be gravitationally bound, the gravitational forces holding the cloud together has to be greater than the forces driving it apart, $|V| > K$. This, along with the density, $\rho = M/(4\pi/3)R^3$, gives the Jeans length,

$$R_{\mathrm{J}} = \left[\frac{15k_{\mathrm{B}}T}{8\pi Gm\rho}\right]^{1/2}, \tag{1.3}$$

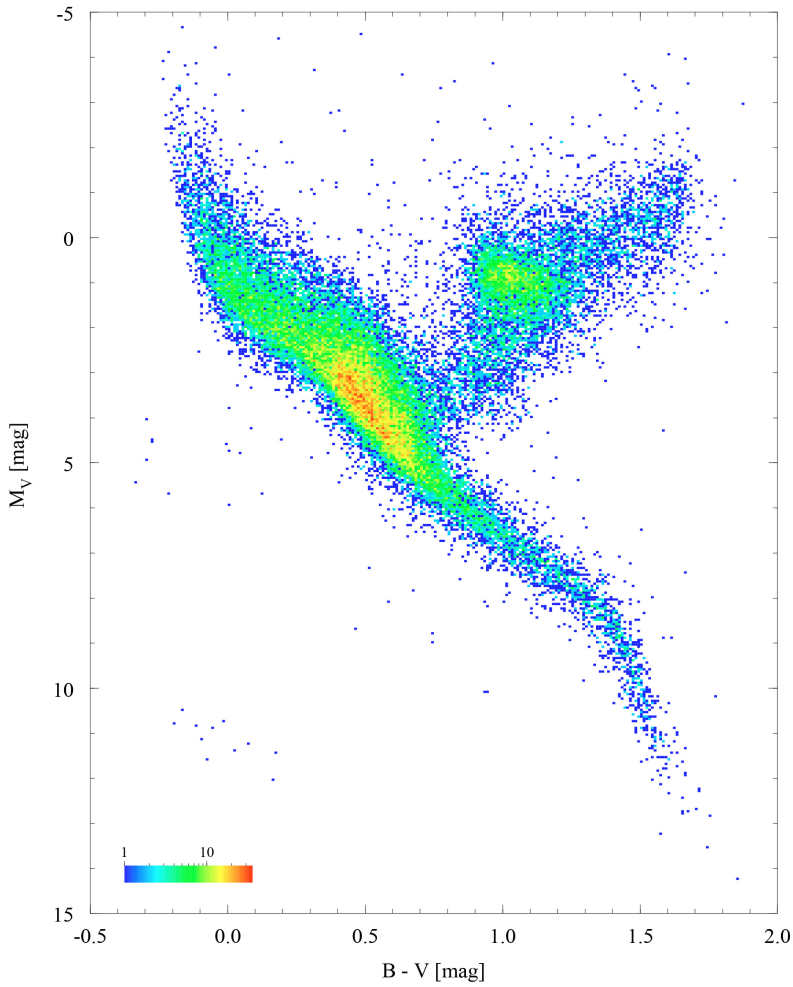

Figure 1.1: HR diagram for 41704 stars from the Hipparcos Catalogue [1].

which is a lower limit for the dimension of a gravitationally bound region. And the Jeans mass,

$$M_{\mathrm{J}} = \frac{4\pi}{3} R_{\mathrm{J}}^3 \rho = \frac{4\pi}{3} \left[\frac{15 k_{\mathrm{B}} T}{8\pi G m} \right]^{3/2} \rho^{-1/2}, \tag{1.4}$$

an upper limit for the mass. Once a cloud becomes gravitationally bound it will begin to collapse. The collapsing region is called a fragment, and will, due to the increased gravitational pull, increase its mass by accretion of surrounding gas. For a bound system, the virial theorem provides a relation between potential energy V

and kinetic energy K, and is given by

$$\langle K \rangle = -\frac{1}{2}\langle V \rangle. \tag{1.5}$$

If the kinetic energy increases, the potential energy decreases. In this case, the potential energy is gravitational, and the kinetic energy is thermal. As material accretes, gravitational energy is released and turned into thermal energy, thus the temperature increases. The temperature will increase until it reaches the threshold for hydrogen ignition, and the star becomes a MS star.
If the cloud is rotating, the collapse is slowed down. This is due to conservation of angular momentum. The angular momentum for a uniform sphere with radius r is $L = (2/5)Mr^2\omega$, where ω is the angular speed. As the cloud collapses, ω increases. Each particle is not only pulled inwards, but also in the direction of the rotation. Thus, the inwards acceleration $a(r) = GM/r^2 - r^2\omega$ is lower compared to a non-rotating cloud. If ω becomes large enough, $\omega = (GM/r^3)^{1/2}$, the rotation can halt the collapse perpendicular to the axis of rotation. Movement parallel to the axis of rotation is unaffected, and the star-forming fragment will flatten, thus making it harder to obtain stellar densities. When it is no longer able to collapse further, it will break up into smaller pieces, where some of them can continue collapsing. This is a possible explanation of the high incidence of binary systems.
Magnetic fields can have an important effect on star formation, as most clouds are sufficiently ionised, making them good conductors. The effect of a magnetic field B becomes important when the associated energy is comparable to the gravitational energy,

$$\left(\frac{B^2}{8\pi}\right)\left(\frac{4\pi}{3}R^3\right) \sim \frac{3}{5}\frac{GM^2}{R}, \tag{1.6}$$

where $B^2/8\pi$ is the magnetic energy density in Gaussian units. As a molecular cloud collapses, the magnetic field strength increases. The charged particles exert a pressure which slows down the collapse. Ions and neutrals might not stay perfectly mixed. As ions drift relative to the neutrals, some of the magnetic flux escape from the cloud. This is called ambipolar diffusion. Sometimes ions collide with neutrals, transferring momentum. This leads to an increase in temperature. Ambipolar diffusion thus serves as a heating source for the cloud, and allows for gradual contraction. This process is thought to produce low mass stars.

1.2 Main-Sequence

A star spends most of its lifetime on the MS. The MS phase is characterised by hydrogen burning in the core. The nuclear energy generated in the core is transported outwards by convection or radiation. The larger the mass of the star, the shorter time the star is in the MS phase.

1.2.1 Nuclear Processes

Depending on the core temperature there are three main nuclear processes taking place in the core during the MS phase, changing the composition of the star. These changes are the reason MS stars forms a band, rather than a thin line, on the HR diagram.

Hydrogen burning I, also known as the proton-proton chain, is the primary source of energy generation. It requires a temperature of 10^7 K. The net result of this chain is that four protons make one helium nucleus (α-particle), in addition to two positrons, two neutrons, and two photons,

$$\begin{aligned} \mathrm{p} + \mathrm{p} &\rightarrow {}^2\mathrm{H} + e^+ + \nu_e \\ {}^2\mathrm{H} + \mathrm{p} &\rightarrow {}^3\mathrm{He} + \gamma \\ {}^3\mathrm{He} + {}^3\mathrm{He} &\rightarrow {}^4\mathrm{He} + 2\mathrm{p}. \end{aligned}$$

The positron will quickly annihilate, heating the gas. The gamma-ray travels a small distance before being absorbed, also heating the gas, while the neutrino escapes completely.

The triple-α process occurs in more massive stars, where the core temperature lies around 10^8 K. This process is especially important at the end of the MS phase. The first step in the chain is

$$ {}^4\mathrm{He} + {}^4\mathrm{He} \rightleftharpoons {}^8\mathrm{Be}. $$

^{8}Be is unstable and will either break up or capture a third α-particle,

$$ {}^4\mathrm{He} + {}^8\mathrm{Be} \rightarrow {}^{12}\mathrm{C} + \gamma. $$

The ^{12}C nucleus works as a catalyst for a third nuclear process:

Hydrogen burning II, the CNO cycle,

$$\begin{aligned} {}^{12}\mathrm{C} + \mathrm{p} &\rightarrow {}^{13}\mathrm{N} + \gamma \\ {}^{13}\mathrm{N} &\rightarrow {}^{13}\mathrm{C} + e^+ + \nu_e \\ {}^{13}\mathrm{C} + \mathrm{p} &\rightarrow {}^{14}\mathrm{N} + \gamma \\ {}^{14}\mathrm{N} + \mathrm{p} &\rightarrow {}^{15}\mathrm{O} + \gamma \\ {}^{15}\mathrm{O} &\rightarrow {}^{15}\mathrm{N} + e^+ + \nu_e \\ {}^{15}\mathrm{N} + \mathrm{p} &\rightarrow {}^{12}\mathrm{C} + {}^4\mathrm{He}. \end{aligned}$$

Here as well, four protons make one ^{4}He nucleus, in addition to two neutrinos, two positrons, and three photons.

1.2.2 Mass Loss

For low-mass stars mass loss is negligible, however, more massive stars lose a significant fraction of their mass during the time spent on the MS. Mass loss takes two forms: continuous stellar winds and sudden ejections of a mass shell, called

superwind. The former is the important one during the MS phase. The wind is generated in the atmosphere of the star, driven by the radiation pressure. The ejected mass $\dot{M}\delta t$ acquires escape velocity $v_{\rm esc}$ by absorbing a fraction f of the momentum carried by the radiation $(L/c)\delta t$. We write

$$\dot{M}\delta t v_{\rm esc} = f\frac{L}{c}\delta t, \tag{1.7}$$

where L is the luminosity and c the light speed. Inserting $v_{\rm esc}^2 = 2GM/R$ we get the mass-loss rate

$$\dot{M} = \left(\frac{f}{2}\frac{v_{\rm esc}}{c}\right)\frac{LR}{GM}. \tag{1.8}$$

1.3 Stellar Old Age

When all the hydrogen in the core has been converted into helium, the MS phase is over. On the HR diagram, the star will move towards the red giant branch. How that happens depends on the mass of the star.

1.3.1 Low Mass Stars

The core temperature in low mass stars ($M < 5M_\odot$) is too low for helium to fuse into heavier elements. This leads to a dynamical instability, the gravitational pull is stronger than the radiation pressure and the core contracts. The temperature now raises until it is sufficiently high for helium burning to take place and the contraction halts.

For stars of mass $M < 2M_\odot$, the core of the star is so dense it becomes degenerate before helium burning starts. Thus the fusion from helium to carbon takes place very fast, resulting in a helium flash, if the mass of the core is about $0.5M_\odot$. The degeneracy is lifted, the core expands and helium burning becomes stable. The temperature in the layer right outside the core increases leading to hydrogen burning in the shell and a separation from the core as it expands. Since the core and the envelope is separate, the core becomes isothermal while the mass increases. However, the mass $M_{\rm c}$ cannot be arbitrarily high. The stability condition is

$$\frac{M_{\rm c}}{M} \lesssim \text{constant}\left(\frac{\mu_{\rm env}}{\mu_{\rm c}}\right)^2, \tag{1.9}$$

where $\mu_{\rm env}$ is the mean molecular weight in the envelope, and $\mu_{\rm c}$ the mean molecular weight in the core. When $M_{\rm c}$ reaches this limit, the core starts to contract. For stars that are more massive than $2M_\odot$, $M_{\rm c}$ already exceeds the condition above, and contracts once the hydrogen is exhausted. The contraction stops when pressure balances gravity.

Meanwhile, the outer layer is heated and expands. Expansion of the gas leads to lower temperature. As the temperature difference between the surface and the interior increases, the energy flow between the two regions increases as well. More photons are then absorbed, which increases the temperature. Thus, the

surface temperature is close to constant, while the luminosity increases due to the expansion. The star has now become a red giant. When the helium in the core has fused into carbon and oxygen, the temperature is too low for further fusion, and the core contracts once again. A helium burning shell develops, and the envelope expands. The outer layers of the red giant are weakly held together. As photons from inside the star are absorbed by the outer layers, their momentum is absorbed as well, causing the shell to move even further outward. This is the second type of mass loss briefly mentioned in section 1.2.2. The shells are thus ejected. The core, which now consists of carbon and oxygen, contracts until the electrons in the core becomes degenerate, turning the core into a white dwarf. As the core contracts the effective surface temperature reaches 30,000 K, and the radiated photons ionize the atoms in the ejected shells, making them shine by fluorescence. The shining envelope is called a planetary nebula. Some stars never reach sufficiently high temperature for helium ignition, they lose their envelope before that stage and leave helium white dwarfs.

1.3.2 Massive Stars

Just as for low mass stars, massive stars also have a helium burning core and a hydrogen burning shell. When the helium in the core is exhausted, carbon and oxygen fuses into even heavier elements. The star then has a carbon and oxygen burning core, a helium burning shell, and a hydrogen burning shell. The core keeps building up heavier elements, and more layers are developed, until the inner core is made of iron group elements. The core is then surrounded by shells of silicone, oxygen, neon, carbon, helium, and a hydrogen rich envelope. The luminosity of the core increases, causing a heating, and thus an expansion of the outer layers. The star becomes a red supergiant. Since iron cannot fuse into heavier elements without spending energy, contraction of the core is inevitable. This will be further discussed in the next chapter.

Chapter 2

Types of Supernovae

Some stars have a more violent death than others. A supernova (SN) is a star undergoing an explosion that briefly outshines an entire galaxy. SNe are divided into two groups, type I and type II. The difference of these is the presence of hydrogen lines in the spectrum. A type I SN shows no hydrogen lines, whereas a type II does.

2.1 Type Ia Supernovae

Type Ia is the most frequent one of the type I SNe. It can occur in close binary systems where one of the stars is a white dwarf. Consider a binary system in a coordinate system rotating with the stars, then draw surfaces with constant effective potential. There are five points, called Lagrangian points, where the effective gravitational force is zero. One of the points, L_1, lies between the stars and connects an equipotential surface shaped as a dumb-bell, see figure 2.1. The volume enclosed is called Roche lobes, and delimits the area in which material is gravitationally bound to only one of the stars. The more massive star will evolve off the MS first, and become a red giant. If the red giant becomes large enough to fill its Roche lobe, some of its mass can be transferred onto the other star, through the point L_1. The star losing mass will eventually become a white dwarf, or an other collapsed object. In the case of a possible type Ia SN it is interesting if the other star also develops into a red giant that fills its Roche lobe. Then mass will transfer back onto the white dwarf. If enough mass falls onto the white dwarf to make its mass greater than the Chandrasekhar limit, $M_{\mathrm{CH}} \approx 1.44 M_{\odot}$, it will collapse. The collapse triggers carbon detonation. The nuclear energy released is greater than the gravitational pull and the white dwarf explodes, leaving no remnant. During the explosion, the temperature rises to the point where a significant amount of ^{56}Ni is created. Later ^{56}Ni decays into ^{56}Co, which then decays into ^{56}Fe.
If the second star is not able to fill its Roche lobe, but instead evolves to a white dwarf, we get a white dwarf binary. The white dwarfs radiate gravitational waves, and in order to make up for the energy loss, the distance between them decreases.

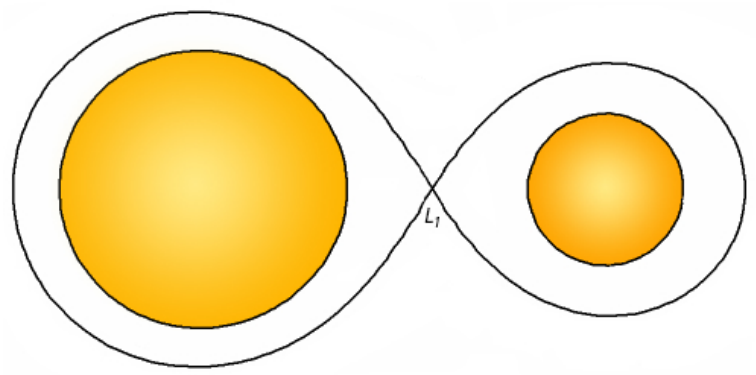

Figure 2.1: Roche lobes for a detached binary system, with L_1 marked.

Eventually, one of them will fill its Roche lobe and accrete material onto the other. The merging of two white dwarfs might result in a type Ia SN [10].

2.1.1 Other Type I Supernovae

Type Ib and Ic are core collapse SNe [11]. The progenitors are massive stars who have lost their hydrogen rich envelope either due to strong winds or a partner in a close binary system. In addition to its hydrogen rich envelope, a type Ic progenitor has also lost its helium shell. The spectral differences can be seen in figure 2.2. The mechanism behind SNe of type Ib/c is more similar to type II than type Ia.

2.2 Type II Supernovae

When a massive star ($M > 10M_\odot$) reaches the end of its time as a MS star it blows up and becomes a red supergiant, see section 1.3.2. The iron core contracts, making the electrons degenerate. When the mass of the degenerate core exceeds the Chandrasekhar limit, the electron degenerate pressure can no longer support the core and it collapses further. During the collapse, some of the energy is released and then absorbed by the iron nucleus, causing the iron to break,

$$^{56}\mathrm{Fe} \rightarrow 13\ ^{4}\mathrm{He} + 4\mathrm{n}.$$

The loss of energy is so severe, that the collapse turns into an almost free fall. This drives the temperature even higher. The photons become energetic enough to break the helium nuclei into protons and neutrons. As the density increases, the liberated protons couple with electrons to create neutrons and neutrinos,

$$e^- + \mathrm{p} \rightarrow \mathrm{n} + \nu_e.$$

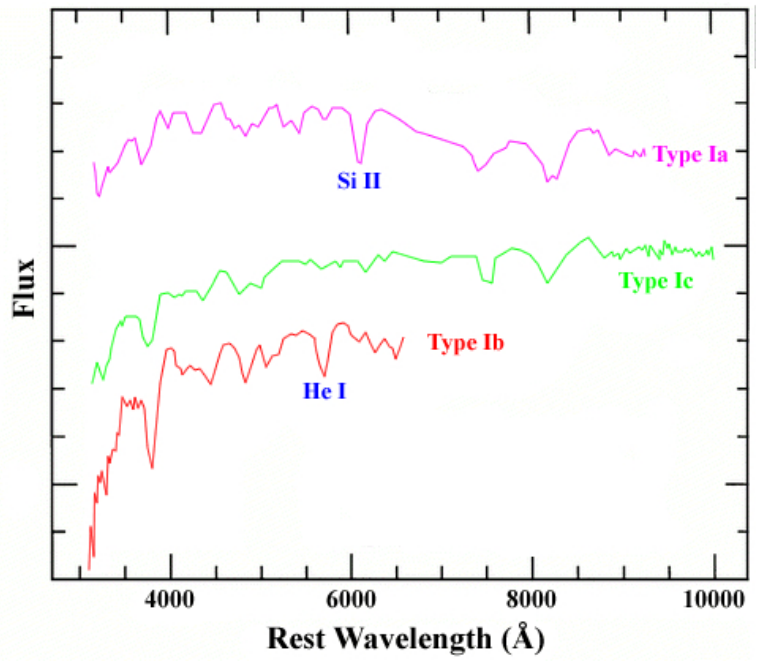

Figure 2.2: The difference in type I SN spectra [2].

The pressure then drops, continuing the collapse until the neutron gas becomes degenerate, at a density around 10^{15} g/cm^3. The collapse results in an explosion where most of the mass of the star is blown away. Exactly how it happens is not well-known. The core is compressed to the point where nuclei starts to overlap. Thus, nuclear forces kick in, and the equation of state stiffens. This can halt the collapse and make the material bounce back, creating a shock wave. The large number of emitted neutrinos (10^{57} for a $10M_\odot$ star [8]) might also have something to do with it. Due to the high density, neutrinos are trapped in the core, creating a neutrinosphere. A significant amount of the neutrino energy is then absorbed by the envelope, giving it a push outwards. During the explosion, heavier elements are created. The remaining degenerate neutron core is classified as a neutron star. If the gravitational pull is larger than the neutron degeneracy pressure, the core will continue to collapse. We do not know of another source of pressure that might halt the collapse, so when radius of the core reaches its Schwarzschild radius,

$$R_\mathrm{S} = \frac{2GM}{c^2}, \tag{2.1}$$

it will become a black hole.

2.2.1 Subclasses of Type II Supernovae

One can separate type II SNe into four subclasses: IIL, IIP, IIn, and IIb [11]. IIL (Linear luminosity decline) and IIP (luminosity Plateau of 2-3 months, then decline) are considered normal type II SN, and refers to the shape of the light curves. These two subclasses are not completely separated, since some cases show a mixture between IIL and IIP. A small subset of type II SNe shows some narrow emission lines, and are classified as type IIn SNe. These lines are most likely due to interaction with dense circumstellar media. A type IIb SN shows similar spectrum as type II SNe at the beginning, but after a while the spectrum resembles that of a type Ib SN, hence the b in IIb.

Chapter 3

Pair-Instability Supernova

Pair-instability (PI) SNe are the most energetic thermonuclear explosions in the universe [6]. The physics of a PI SN is thought to be well-understood: After carbon burning the temperature is so high, $T > 10^9$ K, that electron-positron pairs are created. Thermal pressure drops and the core contracts. This leads to explosive burning of oxygen and silicon. The energy released completely unbinds the star. Whether or not a star is susceptible to PI depends not only on its mass, but on metallicity, mass loss, and mixing due to rotation [12]. Rotation leads to a more chemically homogeneous interior and higher oxygen core masses. A rotating star can therefore encounter PI at lower masses. Higher metallicity means stronger winds and more mass loss. Thus, stars with higher metallicity have to be more massive to die as PI SNe.

3.1 Early Universe

The properties of the first stars are not well known. These first stars are categorized as Population III (Pop III), whereas in the local universe stars are of Pop I (young and metal-rich) or Pop II (old and metal-poor) [8]. Pop III stars are thought to have been born in $10^5 - 10^6\,M_\odot$ dark matter halos [5], either individually or as clusters. Due to the lack of observational data it is hard to predict their masses, but they were probably massive ($15 - 500\,M_\odot$) and extremely metal poor ($Z < 10^{-3.5}\,Z_\odot$). It is believed that the first massive stars ended their life as PI, type IIn, and core collapse (CC) SNe, and that they are the origin of the massive black holes we now find in the centre of galaxies. Another believed consequence of PI SN is the chemical enrichment of the Universe.
The Pop III progenitors of PI SNe are usually in the mass range of 140-260 $M_\odot$ and die as either red hypergiants or blue giants. For stars rotating with a speed of $\sim 50\,\%$ of break up velocity, the mass range is lowered to $90 - 140\,M_\odot$ [6]. They die as compact He cores due to rotational mixing. A slightly less massive star ($\sim 100\,M_\odot$, or $\sim 85\,M_\odot$ if the star is rotating) can also encounter PI [13], but the released energy will fail to completely unbind the star. Instead the star will

shed outer layers in a series of violent ejections. This is called a pulsational pair-instability (PPI) SN. The first ejected shell is usually the most massive one, and is followed by less massive shells with higher velocity. If two shells collide it will be a very luminous event, and might be an explanation to superluminous supernovae such as SN 2006gy. The remaining core will eventually collapse into a neutron star or a black hole. If the mass of the star exceeds 260 $M_\odot$, it will experience PI, but the released energy is consumed by the disintegration of alpha particles into nucleons. Thus the net energy is not enough to halt the collapse, and the star will collapse into a black hole.
The comoving Pop III PI SN rate is estimated to lie between 10^{-8} and $10^{-6}\,\mathrm{yr}^{-1}\,\mathrm{Mpc}^{-3}$, which gives approximately 1 PI SN per 10 SNe in the early universe (redshift $6 \lesssim z \lesssim 25$) [14].

3.2 Local Universe

In the local universe stars have higher metallicities, which means that massive stars will lose most of their mass during their lifetime, and reduce them to compact helium cores. Thus, a local star have to be much more massive in order to explode as a PI SN. The problem with this is the believed upper limit to stellar mass, which were thought to be $\sim 150\,M_\odot$. However, the resent discovery that the star cluster R136 in the Large Magellanic Cloud hosts stars with masses above this limit [4], together with the two candidates SN 2007bi and SN 2213-1745, suggest that PI SNe were not limited to the first stars. A possibility of achieving such massive stars in the local universe is by runaway collisions in young, dense star clusters, which could result in a merged star with sufficient mass [15]. The local PI SN rate is estimated to be $\sim 2 \times 10^{-9}\,\mathrm{yr}^{-1}\,\mathrm{Mpc}^{-3}$, which gives less than one PI SN per ten thousand SNe.

3.2.1 SN 2007bi

SN 2007bi at redshift $z = 0.123$, discovered early in 2007, is classified as a peculiar type Ic supernova. Young et al. [16] compared the light curve of SN 2007bi with other discovered type Ic SNe covering a wide range of properties. SN 2007bi had a peak magnitude of $M \sim -21.3$ mag, which is two magnitudes brighter than the over-luminous SN 1998bw. The light curve also shows a much slower decline compared to the others, which, together with the broad peak, indicate a very large ejected mass. Light curves of type Ic SNe are powered by the decay of ^{56}Ni. The estimated amount of nickel synthesised in the explosion is $M_{Ni} = 3.5 - 4.5\ M_\odot$. Young et al. then argues whether SN 2007bi was a PI or a CC SN, leaning on the latter. Gal-Yam et al. [17] claim, however, that their findings are inconsistent with CC models. They compare the light curve of SN 2007bi to PI SN models, and it is well-fitted for a 100-110 $M_\odot$ helium core. They estimate the amount of nickel to be $\gtrsim 7\ M_\odot$ and the progenitor to have had a helium core with $M \approx 100\ M_\odot$, which could only lead to a PI SN. In comparison, Whalen et al. [4] lists a nickel amount of 9.2 $M_\odot$ associated with a 109 $M_\odot$ helium core for a local PI SN.

3.2.2 SN 2213-1745

Cooke et al. [18] discovered SN 2213-1745 at $z = 2.05$, which is another super-luminous SN with peak magnitude $M \sim -21$ mag in the far-ultraviolet, in a stack of images taken in June - November in 2005 and 2006. They classified it as a SLSN-R, a super-luminous SN with a slowly evolving light curve. The light curve is similar to that of SN 2007bi, both fade slower than any other super-luminous SN. Due to the close agreement, Cooke et al. estimates that they had a similar amount of synthesised ^{56}Ni, and that the progenitor of SN 2213-1745 had an initial mass of $\sim 250\ M_{\odot}$. In their discussion they rule out the possibility of an active galactic nucleus, which can produce similar energies. SN 2213-1745 thus provide the first far-ultraviolet data for a possible PI SN. Cooke et al. also discuss the case SN 1000+0216 at $z = 3.90$, which might have been a PPI or a super-luminous type II SN. However, due to the limiting photometric coverage it is not possible to determine which subclass it belongs to.

Chapter 4

Fluid Dynamics

Most astrophysical objects, e.g. stars, nebulae, and the interstellar medium (ISM), are fluids. Fluid dynamics, the theory of the movement of gases and liquids, therefore plays an important role in many astrophysical problems [19].

4.1 Basic Fluid Equations

A fluid in (local) thermodynamic equilibrium can be completely described by the density, velocity, and temperature of any point in the fluid. The motion of a fluid can then be described with a handful of equations. Consider a fluid element with volume V, density ρ, and velocity $\boldsymbol{u}$. For an ideal fluid, viscosity is neglected.

4.1.1 The Continuity equation

Let the volume V be fixed in space and enclosed by a surface S. The total mass of the fluid element is $\int_V \rho \mathrm{d}V$. The time derivative of this mass is the flux of mass into V across S,

$$\frac{\mathrm{d}}{\mathrm{d}t}\int_V \rho \mathrm{d}V = -\int_S (\rho \boldsymbol{u}) \cdot \boldsymbol{n} \mathrm{d}S, \tag{4.1}$$

where $\boldsymbol{n}$ is a normal vector pointing outward on V. The volume is fixed in space, so it does not matter if we integrate or differentiate first. Using the divergence theorem,

$$\int_V (\boldsymbol{\nabla} \cdot \boldsymbol{F})\, \mathrm{d}V = \int_S \boldsymbol{F} \cdot \boldsymbol{n} \mathrm{d}S, \tag{4.2}$$

we can rewrite equation (4.1):

$$\int_V \frac{\partial \rho}{\partial t} \mathrm{d}V = -\int_V \boldsymbol{\nabla} \cdot (\rho \boldsymbol{u})\, \mathrm{d}V. \tag{4.3}$$

Since the volume V can be chosen arbitrarily, we thus have

$$\frac{\partial \rho}{\partial t} + \boldsymbol{\nabla} \cdot (\rho \boldsymbol{u}) = 0, \tag{4.4}$$

which is the continuity equation.

4.1.2 The Momentum Equation

Assume now that the volume moves with the fluid. The rate of change of the volume (or any other quantity moving with the fluid) with respect to time can then be expressed with the material, or convective, derivative D/Dt:

$$\frac{DV}{Dt} = \frac{\partial V}{\partial t} + \boldsymbol{u} \cdot \boldsymbol{\nabla} V. \tag{4.5}$$

The momentum of the fluid element is $\int_V \rho \boldsymbol{u} \mathrm{d}V$, and its rate of change is the same as the net force acting on the fluid element. There are two types of forces acting on the fluid: body and surface forces. Body forces, e.g. gravity, act on the particles in the fluid element. The net effect is $\int_V \rho \boldsymbol{f} \mathrm{d}V$, where $\boldsymbol{f}$ is the body force per unit mass. Surface forces act normally on the surface with net effect $\int_S -P\boldsymbol{n}\mathrm{d}S$, where P is the pressure. The rate of change of the momentum is then

$$\frac{\mathrm{d}}{\mathrm{d}t}\int_V \rho \boldsymbol{u} \mathrm{d}V = \int_S -P\boldsymbol{n}\mathrm{d}S + \int_V \rho \boldsymbol{f}\mathrm{d}V. \tag{4.6}$$

When we place the time derivative inside the integral, it becomes a material derivative. Since the mass of the fluid is invariant, we get

$$\frac{\mathrm{d}}{\mathrm{d}t}\int_V \rho \boldsymbol{u} \mathrm{d}V = \int_V \rho \frac{D\boldsymbol{u}}{Dt}\mathrm{d}V. \tag{4.7}$$

Eq. (4.6) together with the divergence theorem, eq.(4.2), thus gives

$$\int_V \rho \frac{D\boldsymbol{u}}{Dt}\mathrm{d}V = \int_V (-\boldsymbol{\nabla} P + \rho \boldsymbol{f})\mathrm{d}V. \tag{4.8}$$

Again, the choice of V is arbitrary, so we have that

$$\rho \frac{D\boldsymbol{u}}{Dt} = \rho\left(\frac{\partial \boldsymbol{u}}{\partial t} + (\boldsymbol{u}\cdot\boldsymbol{\nabla})\boldsymbol{u}\right) = -\boldsymbol{\nabla} P + \rho \boldsymbol{f}, \tag{4.9}$$

which is the equation of motion for a fluid.

4.1.3 The Energy Equations

The dot product of the equation of motion, eq. (4.9), with the velocity $\boldsymbol{u}$,

$$\frac{D}{Dt}\left(\frac{1}{2}\boldsymbol{u}^2\right) = -\frac{1}{\rho}\boldsymbol{u}\cdot\boldsymbol{\nabla} P + \boldsymbol{u}\cdot\boldsymbol{f}, \tag{4.10}$$

is the same as the rate of change of the kinetic energy. Equation (4.10) is called the mechanical energy equation.

Let U be the internal energy density. The rate of change of the total energy must be equal to the work done on the fluid plus the rate at which heat is added

to the fluid. Heat can either be generated at a rate ϵ per unit mass within the fluid element (nuclear radiation) or added by the heat flux $\boldsymbol{F}$ across the surface (radiative heat flux)

$$\begin{aligned}\frac{\mathrm{d}}{\mathrm{d}t}\int_V\left(\frac{1}{2}\boldsymbol{u}^2+U\right)\rho\mathrm{d}V=&\int_S\boldsymbol{u}\cdot(-P\boldsymbol{n})\,\mathrm{d}S+\int_V\boldsymbol{u}\cdot\boldsymbol{f}\rho\mathrm{d}V\\&+\int_V\epsilon\rho\mathrm{d}V-\int_S\boldsymbol{F}\cdot\boldsymbol{n}\mathrm{d}S\end{aligned}\tag{4.11}$$

Using eq. (4.2) and the fact that the volume is arbitrarily chosen, we get

$$\rho\left(\frac{D}{Dt}\left(\frac{1}{2}\boldsymbol{u}^2\right)+\frac{DU}{Dt}\right)=-\boldsymbol{\nabla}\cdot(P\boldsymbol{u})+\rho\boldsymbol{u}\cdot\boldsymbol{f}+\rho\epsilon-\boldsymbol{\nabla}\cdot\boldsymbol{F}.\tag{4.12}$$

Subtracting the mechanical energy equation (4.10), we obtain the thermal energy equation

$$\frac{DU}{Dt}=\frac{P}{\rho^2}\frac{D\rho}{Dt}+\epsilon-\frac{1}{\rho}\boldsymbol{\nabla}\cdot\boldsymbol{F}.\tag{4.13}$$

If the system is in thermal equilibrium $\epsilon=(1/\rho)\boldsymbol{\nabla}\cdot\boldsymbol{F}$, and the thermal energy equation is simplified to

$$\frac{DU}{Dt}=\frac{P}{\rho^2}\frac{D\rho}{Dt}.\tag{4.14}$$

4.1.4 The Equation of State

An equation of state (EoS) is a relation between pressure P, temperature T, and density ρ of a system. For an ideal gas the EoS is

$$P=nk_{\mathrm{B}}T,\tag{4.15}$$

where n is the number of particles per volume. We assume first that the stellar gas is an ideal gas. Since there are different species of particles in the stellar gas, the total pressure is the sum of the pressure exerted by the different species: ions, electrons, and photons. The total gas pressure (ions and electrons) is then given by

$$P_{\mathrm{gas}}=P_{\mathrm{I}}+P_e=(n_{\mathrm{I}}+n_e)\,k_{\mathrm{B}}T=\left(\frac{1}{\mu_{\mathrm{I}}}+\frac{1}{\mu_e}\right)\frac{\rho}{m_{\mathrm{H}}}k_{\mathrm{B}}T=\frac{\rho k_{\mathrm{B}}T}{\mu m_{\mathrm{H}}},\tag{4.16}$$

where μ_{I} is the mean atomic mass of stellar material, μ_e^{-1} is the average number of free electrons per nucleon, and m_{H} is the atomic mass unit. The radiation pressure, from photons that transfer momentum to gas particles, is

$$P_{\mathrm{rad}}=\frac{4}{3}\frac{\sigma}{c}T^4,\tag{4.17}$$

where σ is the Stefan-Boltzmann constant. If the gas is degenerate, the EoS is

$$P_{\mathrm{deg}}=K\rho^{\gamma},\tag{4.18}$$

where K is a constant, and γ is the adiabatic exponent. The adiabatic exponent has the value $\gamma=\frac{5}{3}$ for a non-relativistic degenerate gas, and $\gamma=\frac{4}{3}$ for a relativistic degenerate gas. For a more detailed discussion, see [8].

4.1.5 Astrophysical Fluids

For a star, the only body force is due to self-gravity, $\boldsymbol{f} = -\boldsymbol{\nabla}\Phi$. Equations (4.4), (4.9), and (4.13) are then

$$\frac{D\rho}{Dt} + \rho\boldsymbol{\nabla}\cdot\boldsymbol{u} = 0 \tag{4.19}$$

$$\rho\frac{D\boldsymbol{u}}{Dt} + \boldsymbol{\nabla}P + \rho\boldsymbol{\nabla}\Phi = 0 \tag{4.20}$$

$$\frac{DU}{Dt} - \frac{P}{\rho^2}\frac{D\rho}{Dt} - \epsilon + \frac{1}{\rho}\boldsymbol{\nabla}\cdot\boldsymbol{F} = 0. \tag{4.21}$$

These equations, together with the Poisson equation, $\boldsymbol{\nabla}^2\Phi = 4\pi G\rho$, and an EoS, fully describes the system. We assume that ϵ and $\boldsymbol{F}$ are known functions of the other variables. In one spatial dimension these equations can be rewritten to say

$$\partial_t\rho + \partial_x(\rho u) = 0 \tag{4.22}$$

$$\partial_t(\rho u) + \partial_x(\rho u^2 + P) = -\rho\partial_x\Phi \tag{4.23}$$

$$\partial_t\left(\rho\left[\frac{1}{2}u^2 + U\right]\right) + \partial_x\left(\rho u\left[\frac{1}{2}u^2 + U + \frac{P}{\rho}\right]\right) = -\rho\partial_x\Phi + \rho\epsilon - \partial_x F, \tag{4.24}$$

adding the kinetic energy to the last equation.

4.2 Shocks

A shock is a propagating discontinuity caused by e.g. a SN explosion. The shock propagates through matter with a velocity higher than the sound speed. In the following subsections, consider a fluid initially at rest with uniform density ρ_0, pressure P_0, temperature T_0, and internal energy density U_0. Assume thermodynamic equilibrium. Our discussion follow the book by Katz [20].

4.2.1 Sound Waves

Let the fluid undergo a small perturbation,

$$\rho = \rho_0 + \delta\rho \tag{4.25}$$

$$P = P_0 + \delta P \tag{4.26}$$

$$\boldsymbol{u} = \delta\boldsymbol{u}, \tag{4.27}$$

and assume that there are no external forces present. Inserting these new values into equations (4.4) and (4.9), only keeping first order terms in small quantities, we obtain

$$\frac{\partial\delta\rho}{\partial t} + \rho_0\left(\boldsymbol{\nabla}\cdot\delta\boldsymbol{u}\right) = 0 \tag{4.28}$$

$$\frac{\partial\delta\boldsymbol{u}}{\partial t} + \frac{1}{\rho_0}\boldsymbol{\nabla}\delta P = 0. \tag{4.29}$$

Assuming the perturbations are adiabatic, we can reduce the number of variables with

$$\delta P = \left(\frac{\partial P}{\partial \rho}\right) \delta\rho, \tag{4.30}$$

which is analogous to the EoS. Eliminating $\delta \boldsymbol{u}$ from (4.28) and (4.29) by partial derivation with respect to time and to space respectively, gives

$$\frac{\partial^2 \delta\rho}{\partial t^2} = \boldsymbol{\nabla}^2 \delta P = \left(\frac{\partial P}{\partial \rho}\right) \boldsymbol{\nabla}^2 \delta\rho. \tag{4.31}$$

This is the wave equation, $\partial_t \rho = c_\mathrm{s}^2 \boldsymbol{\nabla}^2 \rho$, with $c_\mathrm{s} = \sqrt{(\partial P/\partial \rho)}$ as the adiabatic sound speed. If the perturbations are isothermal, we have $\delta P = a^2 \delta\rho$, where a is the isothermal sound speed. In all cases between adiabatic and isothermal, sound waves are dispersive and damped.

4.2.2 Shocks

Consider now a shock with velocity $\boldsymbol{v}_\mathrm{sh}$ propagating through the fluid. Behind the shock, the fluid has density ρ_1, pressure P_1, velocity $\boldsymbol{u}_1$, temperature T_1, and internal energy density U_1. Everywhere in the fluid, except at the shock, thermal equilibrium holds. In the lab frame the unshocked fluid is at rest. From the conservation laws, which can be easily read from equations (4.22)-(4.24), we find

$$(\rho_1 - \rho_0)\boldsymbol{v}_\mathrm{sh} = \rho_1 \boldsymbol{u}_1 \tag{4.32}$$

$$\rho_0 \boldsymbol{u}_1 \boldsymbol{v}_\mathrm{sh} = P_1 - P_0 \tag{4.33}$$

$$\rho_0 \left(\frac{1}{2}\boldsymbol{u}_1^2 + U_1 - U_0\right) \boldsymbol{v}_\mathrm{sh} = P_1 \boldsymbol{u}_1, \tag{4.34}$$

Eq. (4.32) can be rewritten as $\boldsymbol{u}_1 = \boldsymbol{v}_\mathrm{sh}(\rho_1 - \rho_0)/\rho_1$. Combining this with eq. (4.33), and solving for $\boldsymbol{v}_\mathrm{sh}$ and $\boldsymbol{u}_1$ separately, we find

$$\boldsymbol{v}_\mathrm{sh}^2 = \frac{\rho_1}{\rho_0}\frac{(P_1 - P_0)}{(\rho_1 - \rho_0)}; \qquad\qquad \boldsymbol{u}_1^2 = \frac{(P_1 - P_0)(\rho_1 - \rho_0)}{\rho_1 \rho_0}. \tag{4.35}$$

To keep the solution simple, we assume that the shock propagates at a constant rate. To do this, it is necessary to continually supply energy and momentum from the outside. If this is not done, the shock will gradually weaken, and the solution will be more complex. In the rest frame of the shock, the unshocked fluid has velocity $\boldsymbol{v}_0$ and the shocked fluid has velocity $\boldsymbol{v}_1$. Equations (4.32)-(4.34) then becomes

$$\rho_1 \boldsymbol{v}_1 = \rho_0 \boldsymbol{v}_0 \tag{4.36}$$

$$P_1 + \rho_1 \boldsymbol{v}_1^2 = P_0 + \rho_0 \boldsymbol{v}_0^2 \tag{4.37}$$

$$U_1 + \frac{P_1}{\rho_1} + \frac{1}{2}\boldsymbol{v}_1^2 = U_0 + \frac{P_0}{\rho_0} + \frac{1}{2}\boldsymbol{v}_0^2, \tag{4.38}$$

which yield

$$\boldsymbol{v}_0^2 = \frac{\rho_1}{\rho_0}\left(\frac{P_1 - P_0}{\rho_1 - \rho_0}\right); \qquad \boldsymbol{v}_1^2 = \frac{\rho_0}{\rho_1}\left(\frac{P_1 - P_0}{\rho_1 - \rho_0}\right). \tag{4.39}$$

The three equations (4.36)-(4.38) have four variables on each side, ρ_i, $\boldsymbol{v}_i$, P_i, and U_i. To solve this system of equations, we need an additional constraint in the form of an EoS. Using that of an ideal gas, $P = K\rho^\gamma$, and $\mathrm{d}U = -P\mathrm{d}V$, we get the constraint

$$U_i = \frac{1}{\gamma - 1}\frac{P_i}{\rho_i}. \tag{4.40}$$

Inserting this and eq. (4.39) into eq. (4.38) gives

$$\frac{\gamma}{\gamma - 1}\frac{P_1}{\rho_1} + \frac{1}{2}\frac{\rho_1}{\rho_0}\left(\frac{P_1 - P_0}{\rho_1 - \rho_0}\right) = \frac{\gamma}{\gamma - 1}\frac{P_0}{\rho_0} + \frac{1}{2}\frac{\rho_0}{\rho_1}\left(\frac{P_1 - P_0}{\rho_1 - \rho_0}\right).$$

Multiplying with $\rho_1\rho_0$, collecting terms with γ on one side, and then using the fact that $\left(\rho_1^2 - \rho_0^2\right) = \left(\rho_1 - \rho_0\right)^2 + 2\rho_0\left(\rho_1 - \rho_0\right)$ to make it linear in ρ, we obtain

$$\frac{\gamma}{\gamma - 1}(P_0\rho_1 - P_1\rho_0) = \frac{1}{2}(\rho_1 + \rho_0)(P_1 - P_0).$$

Separating terms with ρ_1 and ρ_0 gives

$$\rho_1\left(P_1 + \frac{\gamma + 1}{\gamma - 1}P_0\right) = \rho_0\left(P_0 + \frac{\gamma + 1}{\gamma - 1}P_1\right).$$

We now have the ratio between ρ_1 and ρ_0:

$$\frac{\rho_1}{\rho_0} = \frac{(\gamma - 1)P_0 + (\gamma + 1)P_1}{(\gamma - 1)P_1 + (\gamma + 1)P_0}. \tag{4.41}$$

For a strong shock, $P_1 \gg P_0$,

$$\frac{\rho_1}{\rho_0} = \frac{V_0}{V_1} \approx \frac{\gamma + 1}{\gamma - 1}, \tag{4.42}$$

so no matter how strong the shock is, it cannot compress matter more than by a factor $(\gamma + 1)/(\gamma - 1)$. This factor is 4 for $\gamma = 5/3$, and 7 for $\gamma = 4/3$.

Chapter 5

Blast Waves

A blast wave is an outward travelling shock produced by an explosion within a fluid [20]. A supernova remnant (SNR) is the result of interaction between the ambient medium and the ejected stellar medium. In the rest frame of the ambient medium a supernova starts off as a point explosion. During the evolution of the SNR, the propagation can be divided into three stages: an ejecta dominated (ED) stage, the Sedov-Taylor (ST) stage, and a radiation dominated stage, also known as the pressure-driven snowplow (PDS) stage. Sometimes the remnant enter a fourth stage, the momentum-conserving snowplow [21] before it merges with the ISM.

The ED stage is initiated when the shock breaks through the outer layer of the stellar progenitor [3]. The ejected material behaves like a piston in the ambient gas, moving with a velocity larger than the sound speed. It is thus preceded by a shock wave, which heats, compresses, and accelerates the ambient medium. The shocked ambient medium pushes back, which results in a reverse shock travelling inwards. The unshocked ejected material expands freely until it is decelerated by the reverse shock. The SNR enters the ST stage when the mass of shocked ambient gas is greater than the mass of ejected material. When most of the ejected energy has been transferred to the ambient medium, the blast wave is adiabatic. Eventually the shock is decelerated to the point where it becomes radiative. The SNR has then entered the PDS stage. A thin shell forms behind the shock front, driven by the pressure of the enclosed hotter shocked ambient medium. As the interior pushes the shell outwards, it loses energy. When all of the thermal energy is lost to radiation, the SNR evolves into the momentum-conserving snowplow stage. At the end of the final stage the shock is weak, propagating nearly at the sound speed. The shell breaks up and the SNR merges with the ISM. Usually this happens before the SNR can evolve into the momentum-conserving snowplow stage.

5.1 Analytic Solution

An analytical one-dimensional approach of the trajectory connecting the first two stages was calculated by Truelove and McKee in 1999 [3]. As a full description is very complex, they had to make certain assumptions. Effects of such as convective instabilities, thermal conduction, magnetic fields, and radiative cooling was neglected. Both the ejected material and the ISM was assumed to be homogeneous. The initial conditions introduced three independent parameters: the ejecta energy E, ejecta mass $M_{\rm ej}$, and the ambient density ρ_0. Combining these by dimensional analysis gives characteristic scales of length and time, which in the case of uniform ambient medium are

$$R_{\rm ch} = M_{\rm ej}^{1/3}\rho_0^{-1/3} = 3.07\left(\frac{M_{\rm ej}}{M_\odot}\right)^{1/3} n_0^{-1/3}\,{\rm pc}, \tag{5.1}$$

$$t_{\rm ch} = E^{-1/2}M_{\rm ej}^{5/6}\rho_0^{-1/3} = 423E_{51}^{-1/2}\left(\frac{M_{\rm ej}}{M_\odot}\right)^{5/6} n_0^{-1/3}\,{\rm yr}. \tag{5.2}$$

Here, n_0 is the ambient hydrogen number density in units of cm^{-3}, and E_{51} is the ejected energy in units of 10^{51} erg. From these characteristic quantities, they defined dimensionless variables $R^* = R/R_{\rm ch}$, $t^* = t/t_{\rm ch}$, and $v^* = v/v_{\rm ch}$, where $v_{\rm ch} = R_{\rm ch}/t_{\rm ch}$. In the case of a non-uniform ambient medium, we have

$$R_{\rm ch} = \left(\frac{M_{\rm ej}}{M_\odot}\right)^{1/(3-s)} \rho_s^{-1/(3-s)}, \tag{5.3}$$

$$t_{\rm ch} = E_{51}^{-1/2}\left(\frac{M_{\rm ej}}{M_\odot}\right)^{[(5-s)/2(3-s)]} \rho_s^{-1/(3-s)}, \tag{5.4}$$

where ρ_s is a normalization constant. A finite ambient mass require $s < 3$. For a stellar wind we have $s = 2$ and $\rho_s = \dot{M}_{\rm w}/\left(4\pi v_{\rm w}\right)$, where $\dot{M}_{\rm w}$ is the mass luminosity of the wind and $v_{\rm w}$ is the wind speed.
The density of the ejected material follow a power-law with index n, $\rho \propto r^{-n}$. A type Ia SN can be described by $n = 7$, a PI SN is assumed to follow either $n = 0$ or $n = 2$. Let $R_{\rm sh}$ be the radius and $V_{\rm sh}$ the velocity of the blast wave. Truelove and McKee's analytical equations for the trajectory of the shock in the ED stage for $n < 3$ is

$$t^*(R_{\rm sh}^*) = \left(\frac{\alpha}{2}\right)^{1/2}\frac{R_{\rm sh}^*}{\ell_{\rm ED}}\left[1 - \frac{3-n}{3}\left(\frac{\phi_{\rm ED}}{\ell_{\rm ED}f_n}\right)^{1/2} R_{\rm sh}^{*3/2}\right]^{-2/(3-n)} \tag{5.5}$$

$$\begin{aligned} V_{\rm sh}^*(R_{\rm sh}^*) = &\left(\frac{2}{\alpha}\right)^{1/2}\ell_{\rm ED} \\ &\times\left(\frac{(1-[(3-n)/3](\phi_{\rm ED}/\ell_{\rm ED}f_n)^{1/2}R_{\rm sh}^{*3/2})^{(5-n)/(3-n)}}{1+(n/3)(\phi_{\rm ED}/\ell_{\rm ED}f_n)^{1/2}R_{\rm sh}^{*3/2}}\right), \end{aligned} \tag{5.6}$$

where $\ell = R_{\rm sh}(t)/R_{\rm r}(t)$, $R_{\rm r}(t)$ is the radius of the reverse shock, ϕ is the ratio of the pressure behind the reverse shock and the blast wave, $\alpha = 2E/M_{\rm ej}v_{\rm ej}^2$, f_n is derived from the structure function $f(v/v_{\rm ej}) = f_n(v/v_{\rm ej})^{-n}$, which describes the time-independent shape of the distribution. For $n < 3$ we have

$$f_n = \frac{3-n}{4\pi}; \qquad \alpha = \frac{3-n}{5-n}. \tag{5.7}$$

The remaining values are listed in table 5.1.

n	$\ell_{\rm ED}$	$\phi_{\rm ED}$	$t^*_{\rm ST}$	$R^*_{\rm ST}$
0	1.10	0.0961	0.495	0.727
2	1.10	0.0947	0.387	0.679
6	1.39	0.39	1.04	1.07
7	1.26	0.47	0.732	0.881

Table 5.1: Parameters for various n from [3].

For $n > 5$, the analytical equations for the ED stage is

$$R^*_{\rm sh}(t^*) = \left\{ \frac{27}{4\pi} \frac{1}{n(n-3)} \frac{\ell_{\rm ED}^{n-2}}{\phi_{\rm ED}} \left[\frac{10}{3} \left(\frac{n-5}{n-3} \right) \right]^{(n-3)/2} \right\}^{1/n} t^{*(n-3)/n} \tag{5.8}$$

$$V^*_{\rm sh}(t^*) = \left(\frac{n-3}{n} \right) \left\{ \frac{27}{4\pi} \frac{1}{n(n-3)} \frac{\ell_{\rm ED}^{n-2}}{\phi_{\rm ED}} \left[\frac{10}{3} \left(\frac{n-5}{n-3} \right) \right]^{(n-3)/2} \right\}^{1/n} t^{*-3/n}, \tag{5.9}$$

where $\ell_{\rm ED}$ and $\phi_{\rm ED}$ is listed in table 5.1 for some $n > 5$.
The ST stage is more straightforward to approximate. Truelove and McKee connected the "classical ST" solution $R_{\rm sh}(t) = (\xi_0 E t^2/\rho_0)^{1/5}$, where $\xi_0 = 2.026$ when $\gamma = 5/3$, to the general ED solution. In terms of dimensionless variables, they got

$$R^*_{\rm sh}(t^*) = [R^{*5/2}_{\rm ST} + \xi_0^{1/2}(t^* - t^*_{\rm ST})]^{2/5} \tag{5.10}$$

$$V^*_{\rm sh}(t^*) = \frac{2}{5}\xi_0^{1/2}[R^{*5/2}_{\rm ST} + \xi_0^{1/2}(t^* - t^*_{\rm ST})]^{-3/5}, \tag{5.11}$$

where $t^*_{\rm ST}$ and $R^*_{\rm ST}$ are the (dimensionless) fiducial transition time and radius, respectively, between the two stages. $t^*_{\rm ST}$ and $R^*_{\rm ST}$ depend on the chosen power-law, n, and are listed in table 5.1 for some n. Figure 5.1 shows the dimensionless trajectories for $n = 0, 2, 6, 7$.
Earlier, in 1988, Cioffi et al. [21] connected the ST stage with the PDS stage in a similar way. The fiducial transition time, radius, and velocity was found to be

$$t_{\rm PDS} \cong 13,300 E_{51}^{3/14} n_0^{-4/7} \zeta_{\rm m}^{-5/14}\,{\rm yr} \tag{5.12}$$

$$R_{\rm PDS} \cong 14 E_{51}^{2/7} n_0^{-3/7} \zeta_{\rm m}^{-1/7}\,{\rm pc} \tag{5.13}$$

$$v_{\rm PDS} \cong 413 E_{51}^{1/14} n_0^{1/7} \zeta_{\rm m}^{3/14}\,{\rm km\,s^{-1}}, \tag{5.14}$$

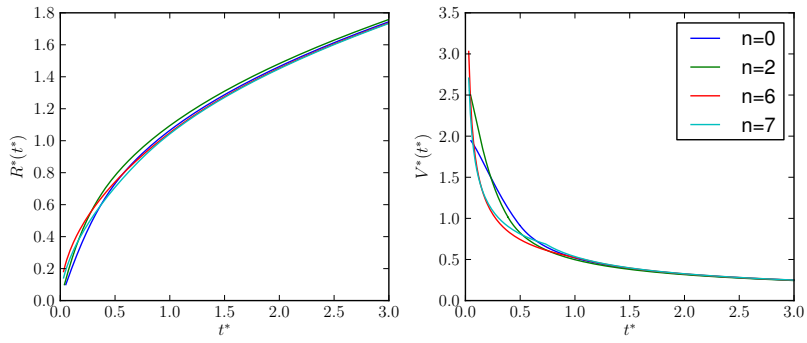

Figure 5.1: Dimensionless shock trajectories for various n.

respectively, where $\zeta_{\rm m}$ is a dimensionless metallicity correction factor of order unity. The expansion equations were estimated to be

$$R_{\rm sh}(t_*) = R_{\rm PDS}\left(\frac{4}{3}t_* - \frac{1}{3}\right)^{3/10} \tag{5.15}$$

$$V_{\rm sh}(t_*) = v_{\rm PDS}\frac{2}{5}\left(\frac{4}{3}t_* - \frac{1}{3}\right)^{-7/10}, \tag{5.16}$$

where $t_* = t/t_{\rm PDS}$.

5.2 Evolution of a PI SNR

To determine the dynamical evolution of a PI SN blast wave, we use the analytical equations from the previous section and values from a series of papers by Whalen et al. [6, 5, 4]. We assume that the shock follows either a $n = 0$ or a $n = 2$ density profile, and insert values from table 5.1. To get the right dimensions, we have to multiply equations (5.5)-(5.6) and (5.10)-(5.11) with the corresponding characteristic values, $V_{\rm sh} = v_{\rm ch} \times V^*_{\rm sh}$, $R_{\rm sh} = R_{\rm ch} \times R^*_{\rm sh}$, and $t = t_{\rm ch} \times t^*$. These values are dependent on the parameters n_0, $M_{\rm ej}$, and E_{51}, and vary between local and Pop III PI SNe.

5.2.1 Local PI SN

A local PI SN can occur in a region with both high and low density, with a number density ranging from $10^{-4}\,{\rm cm}^{-3}$ to $10^{6}\,{\rm cm}^{-3}$. We assume the ISM to be uniform and to have a number density $n_0 = 0.1$ (low) and $n_0 = 10^4$ (high). For a local PI SN we have to account for the mass loss of the progenitor, due to its metallicity and rotation. A star rotating with velocity $v = 0.4\,v_{\rm crit}$, where $v_{\rm crit}$ is the breakup velocity, is assumed to have lost its hydrogen envelope at the onset of PI. A star

with, e.g., initial mass $M = 150\,M_\odot$ will then be reduced to a $109\,M_\odot$ helium core, and a $200\,M_\odot$ star is reduced to $130\,M_\odot$ [4]. At that point the mass is within the mass range for a rotating PI SN, $90 - 140\,M_\odot$, see chapter 3. Some characteristic values can be found in table 5.2.

$M_{\rm ej}/M_\odot$	$n_0(\rm cm^{-3})$	E_{51}	$R_{\rm ch}(\rm pc)$	$t_{\rm ch}(\rm yr)$	$v_{\rm ch}(10^8\rm cm/s)$
109	0.1	42.0	31.6	7013.0	4.41
130	0.1	65.0	33.5	6528.8	5.02
109	10^4	42.0	0.681	151.09	4.41
130	10^4	65.0	0.722	140.66	5.02

Table 5.2: Characteristic values for local PI SNRs in an ISM with different number densities n_0 [4].

In comparison, a $110\,M_\odot$ and a $130\,M_\odot$ Pop III star rotating with $v = 0.5\,v_{\rm crit}$ can explode as a PI SN with ejected energy 39×10^{51} erg and 52×10^{51} erg respectively, see next section. Figure 5.2 shows the trajectories of the shock front in local PI SNe initiated by rotating progenitors with initial masses $150\,M_\odot$ and $200\,M_\odot$. The initial shock velocity is the same in both cases, however, as suspected, the deceleration is greater in the dense medium than in the sparse one. We see that there is no major difference between a $n = 0$ and a $n = 2$ density profile, and will therefore mainly use $n = 2$.

5.2.2 Pop III PI SN

The interstellar medium surrounding Pop III stars is assumed to have a hydrogen number density of $n_0 = (0.1 - 1)\,\rm cm^{-3}$ out to $(100 - 200)\,\rm pc$ [5]. Here, we assume it to be uniform and choose $n_0 = 0.1\,\rm cm^{-3}$. Due to the low metallicity, mass loss is negligible, and the ejected mass is the same as the initial mass. The characteristic values of PI SNe caused by both rotating and non-rotating Pop III stars of different mass and metallicity is then given in table 5.3. Trajectories of the shock front in Pop III PI SNe is shown in figure 5.3.

From figures 5.2 and 5.3 we see that higher metallicity leads to higher shock velocity and larger radius for both non-rotating and rotating progenitors. The difference in velocity and radius seems to be larger for lower masses. Regardless of metallicity and rotation, after 15,000 years, the shock velocity is approximately the same for all cases.

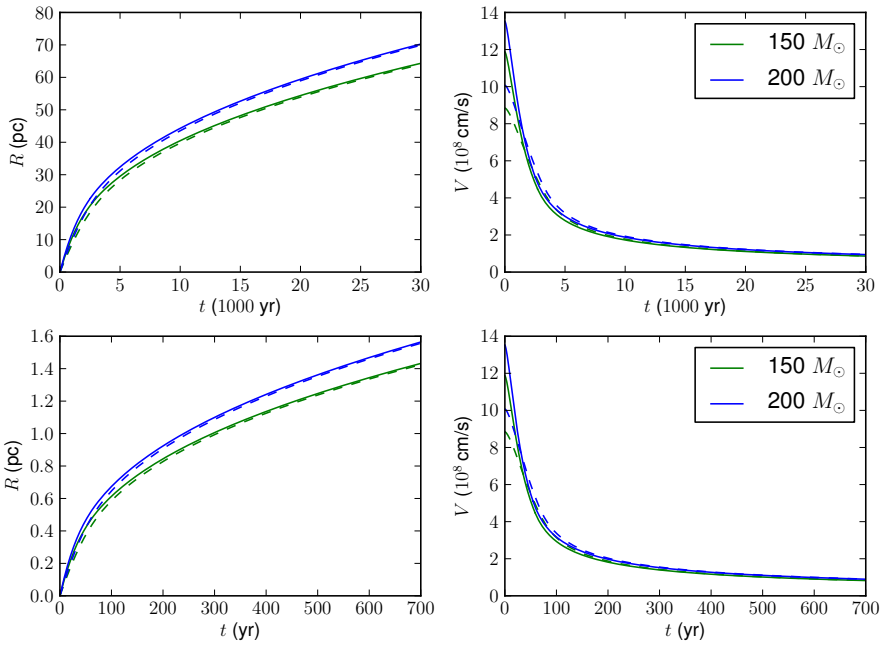

Figure 5.2: Evolution of the shock in a local $150\,M_\odot$ and $200\,M_\odot$ PI SN with a $n = 0$ (dashed) and $n = 2$ (solid) density profile, surrounded by an ISM with number density $n_0 = 0.1$ (upper) and $n_0 = 10^4$ (lower).

$M_{\rm ej}/M_\odot$	$Z(Z_\odot)$	E_{51}	$R_{\rm ch}$(pc)	$t_{\rm ch}$(yr)	$v_{\rm ch}(10^8$cm/s)
150	10^{-4}	9.00	35.1	19768	1.74
175	10^{-4}	21.3	37.0	14611	2.48
200	10^{-4}	33.0	38.7	13120	2.88
225	10^{-4}	46.7	40.2	12167	3.23
250	10^{-4}	69.2	41.7	10912	3.74
175	0	14.6	37.0	17648	2.05
200	0	27.8	38.7	14295	2.65
225	0	42.5	40.2	12754	3.08
250	0	63.2	41.7	11418	3.57
90	0	9.90	29.6	12314	2.35
110	0	39.0	31.7	7333.3	4.23
130	0	52.0	33.5	7299.5	4.49
140	0	80.0	34.3	6959.9	4.82

Table 5.3: Characteristic values for Pop III PI SNRs with progenitors of different masses and metallicities [5] when $n_0 = 0.1$. The bottom three are rotating with $0.5\,v_{\rm crit}$ [6].

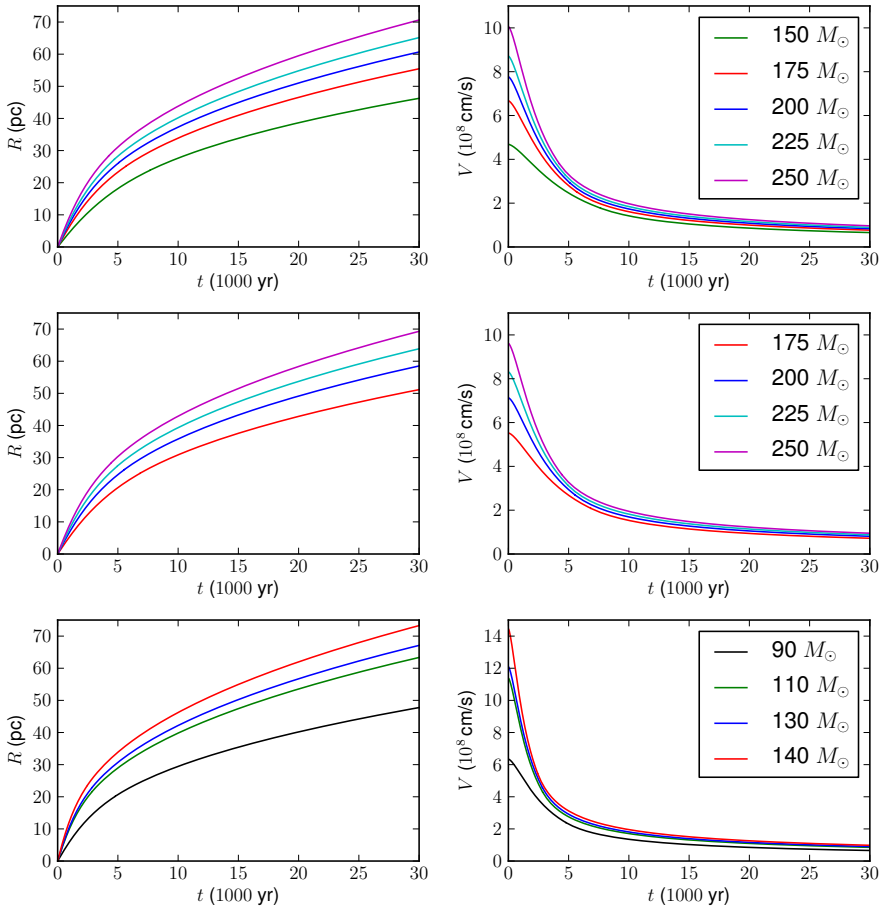

Figure 5.3: Evolution of the shock in a Pop III PI SNR with a $n = 2$ density profile, different masses, and metallicities $Z = 10^{-4}\, Z_\odot$ (upper) and $Z = 0$ (middle), and rotating $Z = 0$ (lower).

Chapter 6

Cosmic Rays

Cosmic rays are high energy particles mostly consistent of protons ($\sim 90\%$[22]), with the rest being alpha particles, heavier nuclei, and electrons. Their origin is not fully known. Most of the cosmic rays entering our atmosphere come from within the Galaxy. The cosmic rays with the highest energies might be of extragalactic origin, produced by active galaxies. In a SN, charged particles can be accelerated to high energies [23] via diffusive shock acceleration. Energetic particles excite Alfvén waves as they stream through the shock front. These waves generates magnetic fluctuations which scatter the particles by random walk. The scattering confines the particles to the vicinity of the shock. This result in first order Fermi acceleration, due to crossing of the shock front several times. The magnetic field is essential for the acceleration to high energies. In a young SNR, the magnetic field is amplified up to 1 mG, which is ~ 100 times more than the average magnetic field in the ISM. This amplification could be due to several instabilities due to, e.g., turbulence driven by a beam of cosmic rays. The ambient magnetic field is tangled and contains loops. The cosmic ray current $\boldsymbol{j}$ interact with these loops, and the loops are stretched with a force $\boldsymbol{j} \times \boldsymbol{B}$. This causes an instability and the magnetic field increases. This instability can increase the magnetic field 100 times its initial value [24].

6.1 Fermi Acceleration

An energetic particle is able to pass the shock front freely, every time it does it gains the relative energy

$$\xi = \frac{E_{k+1} - E_k}{E_k}. \tag{6.1}$$

We want to derive the average energy gain $\langle \xi \rangle$ per encounter. Here one encounter is a pair of one crossing in and one out. The scattering in the pre and post shocked medium works via magnetic field fluctuations and is collisionless. In a simplified picture, consider first a magnetic cloud moving with velocity $V \ll c$ as in the left of figure 6.1. A cosmic ray particle initially with energy E_1 enters the cloud at an

angle θ_1. In the rest frame of the cloud the particle has total energy

$$E_1' = \gamma E_1(1 - \beta\cos\theta_1), \tag{6.2}$$

where $\beta = V/c$ and $\gamma = 1/\sqrt{1-\beta^2}$. Inside the cloud the particle "scatters" on the fluctuations of the magnetic field. The particle exits at an angle θ_2 with an energy

$$E_2 = \gamma E_2'(1 + \beta\cos\theta_2'), \tag{6.3}$$

where E_2' is the energy in the rest frame of the cloud just before it escapes. Since the scattering is collisionless and the cloud is very massive, energy is conserved, $E_2' = E_1'$. The relative energy gain is then

$$\xi = \frac{E_2 - E_1}{E1} = \frac{1 - \beta\cos\theta_1 + \beta\cos\theta_2' - \beta^2\cos\theta_1\cos\theta_2'}{1-\beta^2} - 1. \tag{6.4}$$

To find $\langle\xi\rangle$ we then need $\langle\cos\theta_1\rangle$ and $\langle\cos\theta_2'\rangle$. The probability of a collision is proportional to the relative velocity between the cloud and the particle, and the collision rate is

$$\frac{\mathrm{d}n}{\mathrm{d}\cos\theta_1} = \frac{1}{2}(1 - \beta\cos\theta_1). \tag{6.5}$$

With $-1 \leqslant \cos\theta_1 \leqslant 1$ this gives

$$\langle\cos\theta_1\rangle = \frac{\int \cos\theta_1 \frac{\mathrm{d}n}{\mathrm{d}\cos\theta_1}\mathrm{d}\cos\theta_1}{\int \frac{\mathrm{d}n}{\mathrm{d}\cos\theta_1}\mathrm{d}\cos\theta_1} = -\frac{\beta}{3}. \tag{6.6}$$

Since the particle scatters many times inside the cloud, the exit direction is random so $\mathrm{d}n/\mathrm{d}\cos\theta_2' =$ constant and $\langle\cos\theta_2'\rangle = 0$ when $-1 \leqslant \cos\theta_2' \leqslant 1$. Averaging over eq. (6.4) thus gives

$$\langle\xi\rangle = \frac{1 + \beta^2/3}{1-\beta^2} - 1 \approx \frac{4}{3}\beta^2. \tag{6.7}$$

This is the original, second order, Fermi mechanism [22]. After many encounters there is a net gain of energy, but one encounter could result in either energy gain or loss. Consider now a plane shock front moving with velocity $V \ll c$, as the right hand side of figure 6.1. The relativistic particle crosses the shock front at an angle θ_1, scatters in the shocked medium, and crosses the shock again at an angle θ_2' with an energy E_2. The energies and angles are the same as in the previous case, but now $-1 \leqslant \cos\theta_1 \leqslant 0$ and $0 \leqslant \cos\theta_2' \leqslant 1$. We have

$$\frac{\mathrm{d}n}{\mathrm{d}\cos\theta_1} = 2\cos\theta_1 \quad\text{and}\quad \frac{\mathrm{d}n}{\mathrm{d}\cos\theta_2'} = 2\cos\theta_2', \tag{6.8}$$

which gives $\langle\cos\theta_1\rangle = -2/3$ and $\langle\cos\theta_2'\rangle = 2/3$. Inserted into eq. (6.4) we now get

$$\langle\xi\rangle = \frac{1 + (4/3)\beta + (4/9)\beta^2}{1-\beta^2} - 1 \approx \frac{4}{3}\beta. \tag{6.9}$$

This is the first order Fermi acceleration. The particle always gains energy after an encounter with the shock front. After n acceleration cycles the energy E_n of a

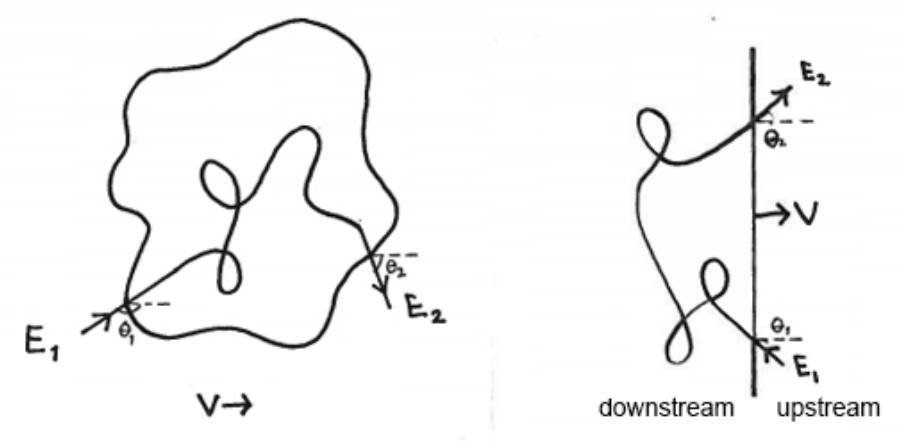

Figure 6.1: Acceleration by a moving cloud (left) and at a shock front (right).

cosmic ray is $E_n = E_0(1+\xi)^n$. Assuming the escape probability $p_{\rm esc}$ is constant, the probability to stay in the region after n cycles is $(1-p_{\rm esc})^n$. The number of particles that are accelerated up to energy E_n is

$$N \propto \sum_{k=n}^{\infty}(1-p_{\rm esc})^k = \frac{(1-p_{\rm esc})^n}{p_{\rm esc}}. \tag{6.10}$$

After inserting $n = \ln(E/E_0)/\ln(1+\xi)$ and some algebra we find

$$N \propto \frac{1}{p_{\rm esc}}\left(\frac{E}{E_0}\right)^{-\alpha}, \tag{6.11}$$

where

$$\alpha = \ln\left(\frac{1}{1-p_{\rm esc}}\right)/\ln(1+\xi). \tag{6.12}$$

When $p_{\rm esc} \ll 1$ and $\xi \ll 1$, we have $\alpha \approx p_{\rm esc}/\xi$. The energy spectrum produced by Fermi acceleration is thus

$$\frac{{\rm d}N}{{\rm d}E} \propto \left(\frac{E}{E_0}\right)^{-(\alpha+1)}. \tag{6.13}$$

Thus, both first and second order Fermi acceleration produces a power-law energy spectrum, which is compatible with the observed spectrum. It can be shown for diffuse shock acceleration that $\alpha \approx 1$.

6.2 Maximum Energy

The number of times a particle crosses the shock front is a random variable, and some particles can achieve very high energies. Since the lifetime of the SN shock

front is finite, the maximum energy a particle can achieve is limited. It is then interesting to know what this maximum energy limit is.
Fermi acceleration of cosmic rays give rise to diffusion in momentum space. The diffusion length cannot be smaller than the gyroradius of the relativistic particle $r_g = E/ZeB$, where Ze is the electric charge of the particle. The smallest diffusion coefficient allowed in the model is then the Bohm diffusion coefficient $\kappa_B = \frac{1}{3} r_g c$ [22, 25]. Let $\boldsymbol{u}_1$ and $\boldsymbol{u}_2$ be the velocity of the upstream and downstream, respectively, of the shock. The acceleration time scale was derived by Drury in 1983 [25] and found to be

$$t_{\mathrm{acc}} = \frac{3}{\boldsymbol{u}_1 - \boldsymbol{u}_2} \left(\frac{\kappa_1}{\boldsymbol{u}_1} + \frac{\kappa_2}{\boldsymbol{u}_2} \right), \tag{6.14}$$

where $\kappa_i \propto 1/B_i$ is the diffusion coefficient on each side of the shock. Let then $\boldsymbol{u}_1 = V_{\mathrm{sh}}$ and $B_1 = B$. The ambient medium has adiabatic compression factor four ($\gamma = 5/3$, see section 4.2.2), so $\boldsymbol{u}_2 = V_{\mathrm{sh}}/4$. If the magnetic field is parallel to the shock front, the field is compressed and $B_2 = 4B$. If the magnetic field is perpendicular to the shock front it is unaffected and $B_2 = B$. We write $4\kappa_1 + 16\kappa_2 = \chi\kappa_B$ so that

$$t_{\mathrm{acc}} = \chi \frac{\kappa_B}{V_{\mathrm{sh}}^2} = \frac{\chi}{3} \frac{cE}{ZeBV_{\mathrm{sh}}^2}, \tag{6.15}$$

where χ is 8 when B is parallel to the shock front and 20 when B is perpendicular. From this, it is easy to show that the energy gain rate from acceleration is

$$\left(\frac{\mathrm{d}E}{\mathrm{d}t} \right)_{\mathrm{acc}} = \frac{3}{\chi} \frac{eBV_{\mathrm{sh}}^2}{c} \tag{6.16}$$

for a proton ($Z = 1$). The adiabatic expansion of the SNR leads to an energy loss which has to be accounted for. From basic dimensional analysis we know that the specific energy E is proportional to pressure P and specific volume V, $E \propto PV$. Combining this with the EoS $P = K\rho^\gamma \propto V^{-\gamma}$ from section 4.1.4 gives $E \propto V^{1-\gamma}$. Derivation with respect to time gives the adiabatic energy loss

$$\left(\frac{\mathrm{d}E}{\mathrm{d}t} \right)_{\mathrm{ad}} = (1 - \gamma) \frac{E}{V} \frac{\mathrm{d}V}{\mathrm{d}t}, \tag{6.17}$$

where V is the volume of the SNR. Since we assume the SNR to evolve spherically, we have that $V = (4/3)\pi R_{\mathrm{sh}}^3$ and $\mathrm{d}V/\mathrm{d}t = 4\pi R_{\mathrm{sh}}^2 V_{\mathrm{sh}}$. Thus

$$\left(\frac{\mathrm{d}E}{\mathrm{d}t} \right)_{\mathrm{ad}} = 3(1 - \gamma) \frac{V_{\mathrm{sh}} E}{R_{\mathrm{sh}}}. \tag{6.18}$$

The maximum proton energy is thus found by solving the differential equation

$$\left(\frac{\mathrm{d}E}{\mathrm{d}t} \right)_{\mathrm{p}} = \frac{3}{\chi} \frac{eBV_{\mathrm{sh}}^2}{c} - 2 \frac{V_{\mathrm{sh}} E}{R_{\mathrm{sh}}}. \tag{6.19}$$

To find the maximum energy a proton can obtain in a PI SNR, we need the results from section 5.2. The dependence of χ and n is shown in figure 6.2 for a non-rotating, zero-metallicity Pop III star with an initial mass of $175\,M_\odot$. Here we

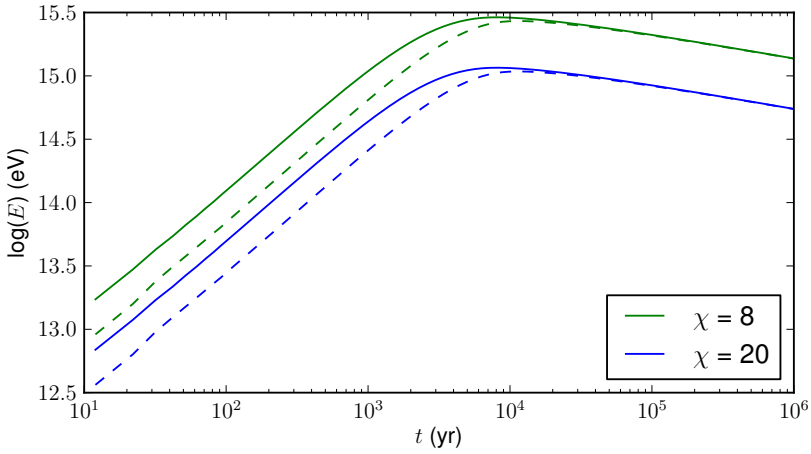

Figure 6.2: χ dependency of the maximum proton energy for a zero-metallicity 175 $M_\odot$ Pop III PI SNR with a $n = 2$ (solid) and $n = 0$ (dashed) density profile.

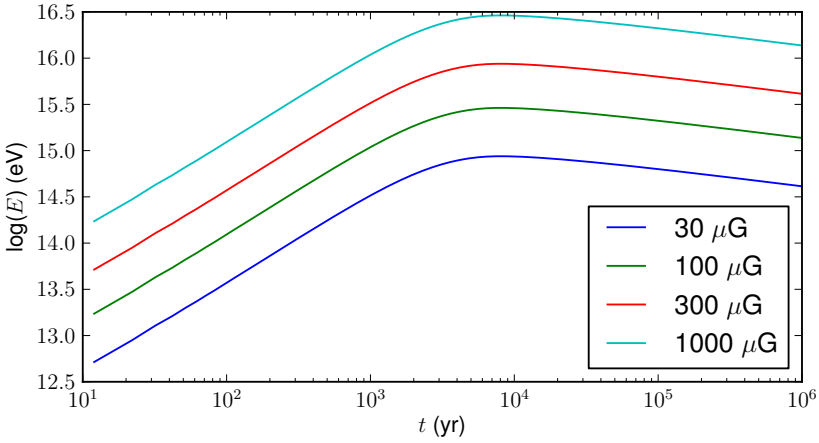

Figure 6.3: Magnetic field B dependency of the maximum proton energy for a zero-metallicity 175 $M_\odot$ Pop III PI SNR with $\chi = 8$ and $n = 2$.

see that the difference between $n = 0$ and $n = 2$ is greater than in section 5.2, as a $n = 2$ density profile result in a maximum energy twice as large as for a $n = 0$ density profile during the first ~ 1000 years. After that, assuming the SNR has not yet merged with the ISM, the adiabatic energy loss is greater than the energy gain, and there is no difference between the two density profiles. The dependence of the

magnetic field B is shown in figure 6.3. Since $(\mathrm{d}E/\mathrm{d}t) \propto B/\chi$, the strength and direction of the magnetic field makes a huge difference in maximum proton energy, as can be seen in figure 6.2 and 6.3. Choosing $\chi = 8$, $n = 2$, and $B = 100\,\mu\mathrm{G}$, the mass dependence is shown in figure 6.4 for both local and Pop III PI SNRs.

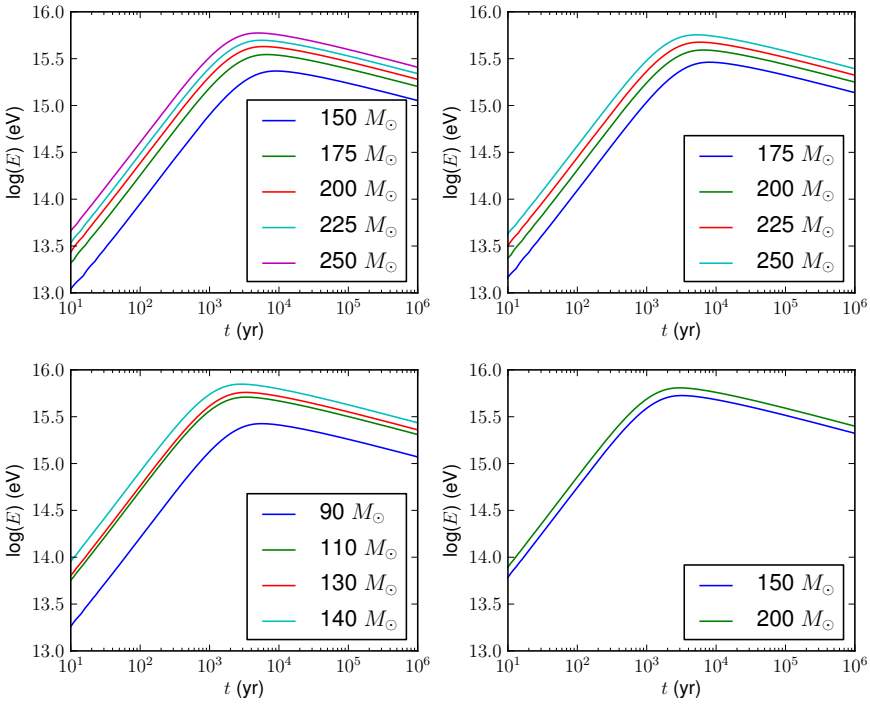

Figure 6.4: Maximum proton energy in PI SNRs caused by non-rotating Pop III stars with metallicity $Z = 10^{-4} Z_\odot$ (upper left) and $Z = 0$ (upper right), rotating Pop III stars (lower left), and local stars (lower right).

Electrons make up around 2 % of cosmic rays and are also accelerated by the Fermi mechanism. To find the maximum energy of an electron we have to consider energy loss from effects such as synchrotron radiation and inverse Compton scattering. The maximum electron energy is briefly discussed in appendix A.

6.3 Secondary Particles

The production of secondary particles, or just secondaries, occurs when cosmic ray particles collide with particles of the ISM near the source [22]. Secondaries are created in hadronuclear (pp) and photohadronic (pγ) reactions. Around the SNR

pp interactions are the main source for secondary particles. The interaction rate for a high energy proton colliding inelastically with a proton at rest is $P_{pp} = \sigma_{pp} n_0 c$, where σ_{pp} is the proton-proton inelastic cross section [26]. σ_{pp} depends on the energy of the moving proton, and thus the center of mass energy $(2Em_{\mathrm{p}})^{1/2}$, and lies in the range of $(30 - 75)\,\mathrm{mb}$ [7]. The collision will produce new particles, most of which are unstable and decay quickly, mainly pions. Due to their short lifetime, pions decay before they interact further,

$$\pi^0 \to 2\gamma \tag{6.20}$$

$$\pi^{\pm} \to \mu^{\pm} + \nu_{\mu}(\bar{\nu}_{\mu}). \tag{6.21}$$

Muons have a very small interaction cross section, and will decay as

$$\mu^{\pm} \to e^{\pm} + \nu_e(\bar{\nu}_e) + \bar{\nu}_{\mu}(\nu_{\mu}), \tag{6.22}$$

and we are left with photons, electrons, positrons, and neutrinos. The electrons and positrons of different muon decays might annihilate, adding more photons. The resulting neutrinos will have typical energies around $0.04E_p$ [27].
pγ-secondaries are produced when cosmic rays collide with background photons [26],

$$\gamma + \mathrm{p} \to \mathrm{n} + \pi^+ \tag{6.23}$$

$$\gamma + \mathrm{p} \to \mathrm{p} + \pi^0. \tag{6.24}$$

The pions decay as previously stated, and $\mathrm{n} \to \mathrm{p} + e^- + \bar{\nu}_e$.
The source function of a secondary particle of type i is given by [22]

$$q_i(E) = \frac{4\pi\rho}{m} \int \mathrm{d}E' \frac{\mathrm{d}\sigma(E, E')}{\mathrm{d}E} \frac{\mathrm{d}N}{\mathrm{d}E'}, \tag{6.25}$$

where E is the energy of the secondary, E' the energy of the primary, and $\mathrm{d}\sigma(E, E')/\mathrm{d}E$ is the differential cross section.

6.4 Cosmic Ray Flux

The cosmic ray flux from PI SNe is found via the cosmic ray energy spectrum, which is given by

$$\frac{\mathrm{d}N}{\mathrm{d}E} = N_0 \left(\frac{E}{E_0}\right)^{-\Gamma}, \tag{6.26}$$

where $\Gamma = \alpha + 1$ in eq. (6.13), N_0 is a normalization constant, and E_0 is an arbitrarily chosen reference energy, e.g. the rest energy of a relativistic proton $m_p c^2 \approx 1\,\mathrm{GeV}$. To determine N_0 we need to know the total energy E_{CR} that goes into cosmic rays, which we assume to be 10 % of the total ejected energy. Then we have that

$$E_{\mathrm{CR}} = \int_{E_0}^{E_{\max}} \mathrm{d}E E \frac{\mathrm{d}N}{\mathrm{d}E}, \tag{6.27}$$

where $E_{\max}$ is the maximum proton energy found in 6.2, $E_{\max} \sim 4 \times 10^{15}\,\mathrm{eV}$ seems to be a good representation. A PI SN with a $175\,M_\odot$ non-rotating, zero-metallicity progenitor will have cosmic ray energy $E_{\mathrm{CR}} = 1.46 \times 10^{51}\,\mathrm{erg}$, and a rotating $110\,M_\odot$ progenitor will have $E_{\mathrm{CR}} = 3.9 \times 10^{51}\,\mathrm{erg}$, see section 5.2. From this we find N_0 to be

$$N_0 = (2-\Gamma)\frac{E_{\mathrm{CR}} E_0^{-\Gamma}}{E_{\max}^{2-\Gamma} - E_0^{2-\Gamma}} \approx (\Gamma - 2) E_{\mathrm{CR}} E_0^{-2}. \tag{6.28}$$

We insert N_0 into the spectrum in eq. (6.26) and obtain

$$\frac{\mathrm{d}N}{\mathrm{d}E} = (2-\Gamma)\frac{E_{\mathrm{CR}} E^{-\Gamma}}{E_{\max}^{2-\Gamma} - E_0^{2-\Gamma}} \approx (\Gamma - 2) E_{\mathrm{CR}} E^{-\Gamma} E_0^{\Gamma-2}. \tag{6.29}$$

The intensity $I(E)$ of cosmic rays is proportional to the number density $n(E)$ of relativistic cosmic rays, $I(E) = (c/4\pi)n(E)$ [28]. We assume the PI SNe to emit cosmic rays isotropically. The total intensity of cosmic rays from every PI SNe throughout the history of the Universe is then given by

$$I_{\mathrm{CR}}(E) = \frac{c}{4\pi} \int_{z_0}^{z_{\max}} \frac{\mathrm{d}z}{H(z)(1+z)} \dot{n}(z) \frac{\mathrm{d}N}{\mathrm{d}E}(E' = E(1+z)), \tag{6.30}$$

where $\dot{n}$ is the SN rate, and $H(z) \approx 72[0.68 + 0.32(1+z)^3]^{1/2}\,\mathrm{km\,s^{-1}\,Mpc^{-1}}$ is the Hubble parameter as a function of redshift, see appendix B.
The Pop III PI SN rate $\dot{n}_{\mathrm{PISN}}$ can be found via the star formation rate (SFR) [14]

$$\dot{n}_{\mathrm{PISN}}(z) = \mathrm{SFR}(z) \frac{\int_{\mathrm{PISN}} \mathrm{d}\log M \psi(M)}{\int_{\mathrm{PopIII}} \mathrm{d}\log M M \psi(M)}, \tag{6.31}$$

where $\psi(M)$ is the Pop III initial mass function. The masses of Pop III stars range from $(5-500)\,M_\odot$ and stars of $(140-260)\,M_\odot$, or $(90-260)\,M_\odot$ if we include rotating stars, die as PI SNe (see chapter 3). The SFR of Pop III stars is first assumed to be constant through time and is estimated to be $10^{-4} M_\odot\,\mathrm{yr^{-1}Mpc^{-3}}$ [14], and we assume a Salpeter slope for the initial mass function $\psi(M) \propto M^{-1.35}$ [29]. If we only include non-rotating stars, we get $\dot{n}_{\mathrm{PISN}} \approx 7 \times 10^{-8}\,\mathrm{yr^{-1}\,Mpc^{-3}}$. The flux of cosmic rays is then plotted as $E^2 I_{\mathrm{CR}}(E)$ in figure 6.5 for different Γ's. Since not much is known of these first stars, it might be better to look at a flux range. The Pop III SFR is estimated to range between $10^{-5} - 10^{-3}\,M_\odot\,\mathrm{yr^{-1}\,Mpc^{-3}}$ up to $z = 6$ [30]. Including rotating stars, the flux range is shown in figure 6.6 for a mean magnetic field of $B = 100\,\mu\mathrm{G}$ and $\Gamma = 2.2$.
A different approach to find the flux is to look at PI SNe as if the SNe happens in a galaxy like the star burst galaxy M82 or the Milky Way. For this we need to know the SFR and cosmic ray luminosity L_{CR} of these galaxies. We then find the luminosity density $Q_{\mathrm{CR}} = L_{\mathrm{CR}}/V$, where V is the volume, corresponding to a SFR of $1\,M_\odot\,\mathrm{yr^{-1}\,Mpc^{-3}}$. We then have

$$Q_{\mathrm{CR}} = \dot{n} \int_{E_0}^{E_{\max}} \mathrm{d}E E \frac{\mathrm{d}N}{\mathrm{d}E} = \frac{\dot{n} N_0 E_0^\Gamma}{2-\Gamma}\left(E_{\max}^{2-\Gamma} - E_0^{2-\Gamma}\right) \approx \frac{\dot{n} N_0}{\Gamma - 2} E_0^2, \tag{6.32}$$

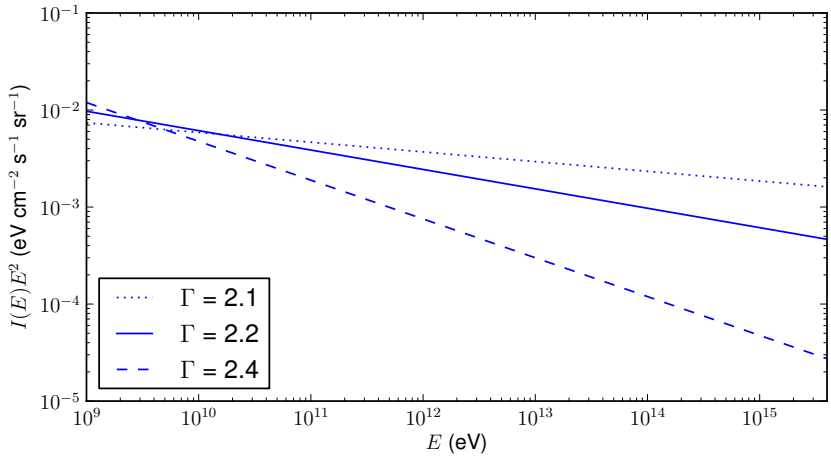

Figure 6.5: Cosmic ray flux from Pop III PI SNRs with different energy spectrum slopes Γ.

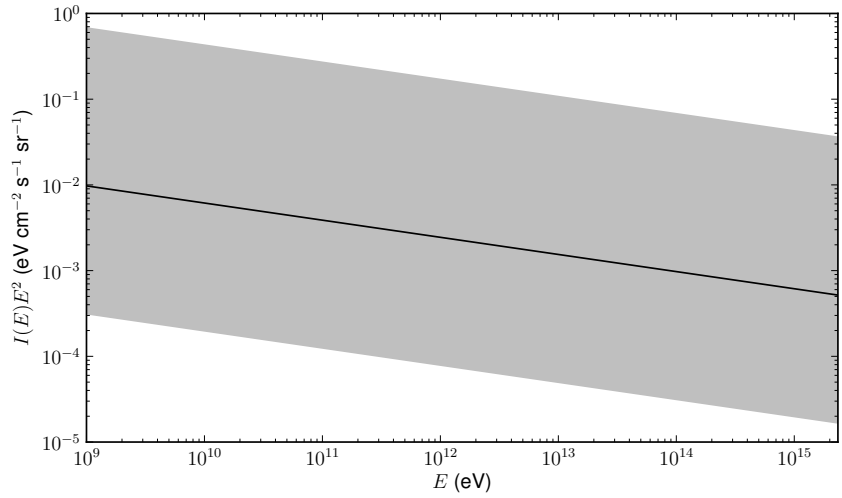

Figure 6.6: Flux range for cosmic rays accelerated in Pop III PI SNRs. The middle black line is the previously calculated flux.

which implies that $\dot{n} \approx (\Gamma - 2)Q_{\rm CR}/N_0 E_0^2$. We define $q_{\rm CR} \equiv \dot{n}(\mathrm{d}N/\mathrm{d}E)$, insert $\dot{n}$, and obtain

$$q_{\rm CR} = \frac{Q_{\rm CR}}{E_0^2/(\Gamma - 2)} \left(\frac{\rm SFR}{1 M_\odot \mathrm{yr}^{-1} \mathrm{Mpc}^{-3}} \right) (E/E_0)^{-\Gamma}. \tag{6.33}$$

To compare this to the first approach we switch $\dot{n}(\mathrm{d}N/\mathrm{d}E)$ with $q_{\rm CR}$ in equation (6.30),

$$I(E) = \frac{c}{4\pi} \int_{E_0}^{E_{\rm max}} \frac{\mathrm{d}z}{H(z)(1+z)} q_{\rm CR}(E'), \tag{6.34}$$

with $E' = E(1+z)$, and insert the Pop III SFR.

M82 has a SFR of $8\,M_\odot$/yr and $L_{\rm CR} \approx 2 \times 10^{40}\,\mathrm{erg/s}$ [31], which gives

$$Q_{\rm CR} = \frac{2 \times 10^{40}\,\mathrm{erg/s}}{8\,\mathrm{Mpc}^3} = 5 \times 10^{-23}\,\mathrm{eV\,cm^{-3}\,s^{-1}}. \tag{6.35}$$

The Milky Way has SFR$= 2\,M_\odot$/yr [31] and $L_{\rm CR} \approx 8 \times 10^{40}\,\mathrm{erg/s}$ [32], which gives

$$Q_{\rm CR} = \frac{8 \times 10^{40}\mathrm{erg/s}}{2\,\mathrm{Mpc}^3} = 8 \times 10^{-22}\,\mathrm{eV\,cm^{-3}\,s^{-1}}. \tag{6.36}$$

Inserted into eq. (6.33) with SFR$= 10^{-4}\,M_\odot \mathrm{yr}^{-1}\,\mathrm{Mpc}^{-3}$ and $\Gamma = 2.2$, and plotted as $E^2 I(E)$ in figure 6.7 together with the one found earlier. From this is seems like the first approach might be an overestimate, especially considered that not all Pop III stars die as PI SNe.

6.4.1 Neutrino Flux

The neutrino intensity is proportional to the proton intensity, and is given by

$$I_\nu(E) = f_{\rm int}(E) Y_\nu(E, \Gamma) I_{\rm CR}(E), \tag{6.37}$$

where $f_{\rm int}(E)$ is the interaction probability and $Y_\nu(E, \Gamma)$ is the yield. Formally $Y_\nu(E, \Gamma)$ is the number of neutrinos produced by one proton with the same energy, colliding inelastically with another proton. The yields used here are energy independent and listed in table 6.1 for different Γ's. For a low number density $n_{\rm s}$ in the SNR, $f_{\rm int}(E) = c n_{\rm s} \sigma_{\rm pp} \tau_{\rm esc}$ is the average number of collisions experienced by one proton, where $\tau_{\rm esc}$ is the average escape time. In higher densities, when $f_{\rm int} > 1$, we have that $f_{\rm int} \approx 1/(1 - 0.5^{\Gamma - 1}) = 1.77$, when $\Gamma = 2.2$.

Due to neutrino oscillations, it is not necessary to distinguish between different species of neutrinos. We therefore consider every neutrino specie as one, and use only Y_ν from table 6.1. The neutrino flux is then plotted in figure 6.8, comparing it to the proton flux, when $\Gamma = 2.2$ and $f_{\rm int} = 1$. From figure 6.8, we see that the

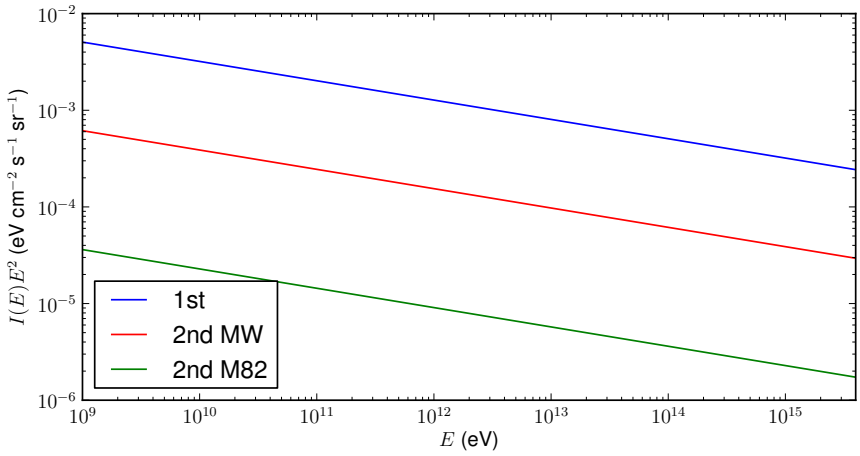

Figure 6.7: Cosmic ray flux estimated by different approaches: Cosmic ray energy is 10 % of ejected energy (1st), all Pop III PI SNe happened in a galaxy like the Milky Way (2nd MW) or M82 (2nd M82).

Γ	2.1	2.2	2.3	2.4	2.5
ν_e	35.1	26.3	19.5	14.5	11.0
$\bar{\nu}_e$	23.6	17.7	12.8	9.31	6.87
ν_μ	63.1	47.3	34.9	26.0	19.6
$\bar{\nu}_\mu$	63.1	47.3	34.9	25.9	19.5
Y_ν	185	139	102	75.7	57.0

Table 6.1: Yields $Y(\Gamma) \times 10^3$ of pp neutrinos with $Y_\nu = \sum_{\nu_i} Y_{\nu_i}$ [7].

diffuse neutrino flux from Pop III PI SNRs is less than $10^{-3}\,\mathrm{eV\,cm^{-2}\,s^{-1}sr^{-1}}$, and therefore they contribute less than 0.01 % to the isotropic neutrino background, which is $\sim 10\,\mathrm{eV\,cm^{-2}\,s^{-1}sr^{-1}}$ [27]. Looking at figure 6.6 we see that even the upper limit of the proton flux from Pop III PI SNe is below this value, and then the neutrinos contributes less than 1 % to the diffuse background flux.
The same amount of energy goes into photons, however, photons scatter off of the background, and are harder to track. Therefore they will not be considered here.

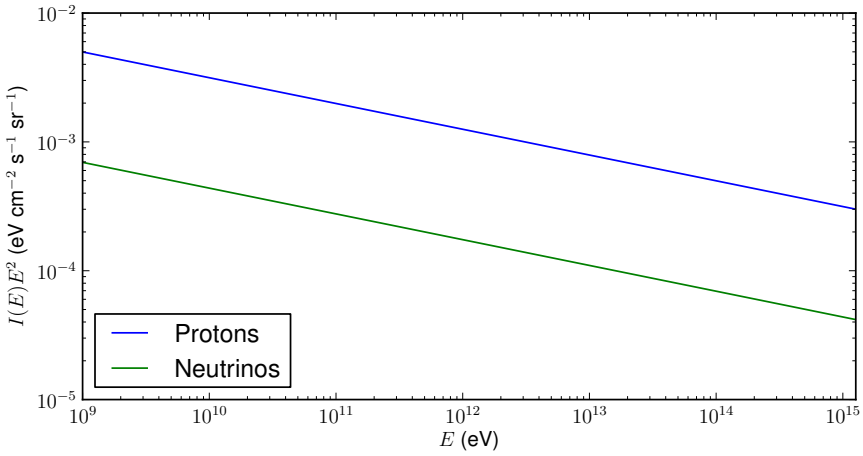

Figure 6.8: The pp neutrino flux compared to the proton flux when $f_{\text{int}} = 1$.

Chapter 7

Conclusion and Outlook

In this thesis we have considered an analytical set of equation, developed by Truelove and McKee, to determine the dynamical evolution of a SN blast wave. We have then used data obtained by several numerical simulations preformed by Whalen et al. to see how a PI SN blast wave propagates. We have looked at how cosmic rays are accelerated to high energies in the SNR, and the maximum energy they can achieve. The maximum energy depended heavily on the magnetic field around the shock front, and was found to be 4×10^{15} eV for a mean magnetic field of $100\,\mu$G. Assuming that the SNR has not merged with the ISM within a few thousand years, the adiabatic energy loss will eventually be greater than the energy gain. We looked at secondary cosmic rays, and found the diffusive neutrino flux, which is sub-dominate, contributing less than 1 % to the neutrino background.

If more time was available it would be interesting to look at the propagation of a SNR through a stellar wind ($s = 2$). This would be most relevant for local stars that experience mass loss due to stellar winds at the end of their lifetime. Another possibility would be to estimate the photon flux. As photons interact with the background, initiating electromagnetic cascades, it would require more work.

There are still a lot of unanswered questions when it comes to the first stars, after all, no Pop III stars have been observed so far. All data used in this thesis are from numerical simulations, and the expected mass range depend on which model is used. No models can constrain the Pop III initial mass function. In this thesis we used a Salpeter slope, but there are some speculations that a top-heavy initial mass function would be a better fit. A different initial mass function could rise or lower the diffuse flux found here. Future near-infrared missions like the James Webb Space Telescope (JWST) and the Wide-Field Infra-red Survey Telescope (WFIRST) are expected to detect Pop III PI SNe, and thus give a deeper understanding about both Pop III stars and PI SNe.

Appendix A

Maximum Electron Energy

Electrons are accelerated in a SNR in the same way as protons in section 6.2. However, due to the electron's light mass effects such as bremsstrahlung, which are negligible for protons, and inverse Compton scattering have to be accounted for. Bremsstrahlung is electromagnetic radiation produced when a charged particle accelerates [33]. Synchrotron radiation is a special case of bremsstrahlung, and leads to an energy loss

$$\left(\frac{\mathrm{d}E}{\mathrm{d}t}\right)_{\text{synch}} = -\frac{4}{3}\frac{\sigma_{\mathrm{T}}E^2U_{\mathrm{B}}}{m^2c^3} = -\frac{\sigma_{\mathrm{T}}B^2E^2}{6\pi m^2c^3}, \tag{A.1}$$

where $\sigma_{\mathrm{T}} = 6.65 \times 10^{-25}\,\mathrm{cm}^2$ is the Thompson scattering cross section. Inverse Compton scattering is when an electron scatter off of a photon. The electron loses energy, and the energy loss rate is given by

$$\left(\frac{\mathrm{d}E}{\mathrm{d}t}\right)_{\text{IC}} = -\frac{4}{3}\frac{\sigma_{\mathrm{T}}E^2U_{\mathrm{ph}}}{m^2c^3}, \tag{A.2}$$

where U_{ph} is the photon energy density. The maximum electron energy is thus found by solving

$$\left(\frac{\mathrm{d}E}{\mathrm{d}t}\right)_{e} = \frac{3}{\chi}\frac{eBV_{\mathrm{sh}}^2}{c} - 2\frac{V_{\mathrm{sh}}E}{R_{\mathrm{sh}}} - \frac{4}{3}\frac{\sigma_{\mathrm{T}}E^2}{m^2c^3}\left(\frac{B^2}{8\pi} + U_{\mathrm{ph}}\right). \tag{A.3}$$

For $U_{\mathrm{ph}} = 0.6\,\mathrm{eV\,cm}^{-3}$, the maximum electron energy obtained in a typical PI SNR is shown in figure A.1 for different magnetic field strengths.

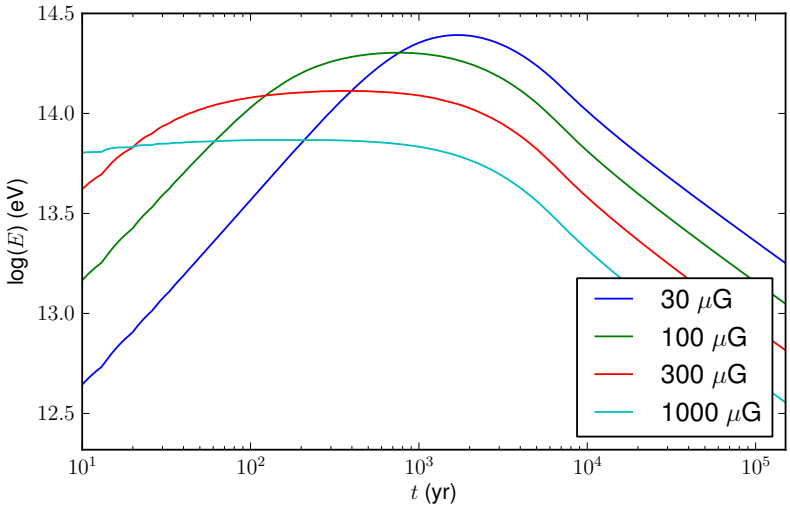

Figure A.1: Maximum electron energy for different magnetic field strengths.

Appendix B

Cosmology

Assume the Universe to be homogeneous and isotropic. The geometry of the Universe is then described by the Friedmann-Robertson-Walker metric [34]

$$\mathrm{d}s^2 = \mathrm{d}t^2 - R^2(t)\left[\frac{\mathrm{d}r^2}{1-kr^2} + r^2(\sin^2\vartheta)\mathrm{d}\phi^2 + \mathrm{d}\vartheta^2\right], \tag{B.1}$$

where $k \in \{-1, 0, 1\}$ specifies the curvature ($k = 0$ flat, $k = \pm 1$ positive/negative curvature), and $R(t)$ is a scale factor. The equations of motion for the Universe is derived from Einstein's field equation

$$R_{\mu\nu} - \frac{1}{2}g_{\mu\nu}R = 8\pi G T_{\mu\nu} + \Lambda g_{\mu\nu}, \tag{B.2}$$

where Λ is the cosmological constant, $g_{\mu\nu}$ is the space-time metric described by eq. (B.1), and

$$T_{\mu\nu} = -P g_{\mu\nu} + (P + \rho)v_\mu v_\nu \tag{B.3}$$

is the energy-momentum tensor for a perfect fluid with pressure P, energy density ρ, and co-moving velocity $v = (1, 0, 0, 0)$. From eq. (B.2) and (B.3) we find the Friedmann equation

$$H^2 = \left(\frac{\dot{R}}{R}\right)^2 = \frac{8\pi}{3}G\rho - \frac{k}{R^2} + \frac{\Lambda}{3}, \tag{B.4}$$

where H is the Hubble parameter, and the "acceleration equation"

$$\frac{\ddot{R}}{R} = \frac{\Lambda}{3} - \frac{4\pi G}{3}(\rho + 3P), \tag{B.5}$$

which determines the acceleration (or deceleration) of the Universe. As matter has $\rho > 0$ and $P \geq 0$, the Universe cannot be static when $\Lambda = 0$, and since $\dot{R} > 0$, the Universe has a finite age. If we let $k = 0$ and $\Lambda = 0$ in the Friedmann eq., we find a critical density

$$\rho_{\mathrm{crit}} = \frac{3H^2}{8\pi G}, \tag{B.6}$$

which can be used to define cosmological density parameters $\Omega_i = \rho_i/\rho_{\rm crit}$. We distinguish between the different contributions to the total density, and define the density parameter for relativistic particles $\Omega_{\rm r}$, for the vacuum $\Omega_{\rm v}$, and for pressureless matter $\Omega_{\rm m}$. With present day values, eq. (B.4) can be rewritten as

$$\frac{k}{R_0^2} = H_0^2(\Omega_{\rm m} + \Omega_{\rm r} + \Omega_{\rm v} - 1). \tag{B.7}$$

With $\Lambda = 8\pi G\rho_\Lambda \neq 0$ the cosmological constant acts as a constant energy density with density parameter $\Omega_\Lambda = \Lambda/(3H^2)$. Inserted into equation (B.5)

$$\frac{\ddot{R}}{R} = \frac{8\pi G}{3}\rho_\Lambda - \frac{4\pi G}{3}(\rho + 3P), \tag{B.8}$$

we see that Λ is equivalent to matter with an EoS $w = P/\rho = -1$.
For observational cosmology, we have to account for the expansion of the Universe. As the Universe expands, the wavelength λ of photons expand by the same proportion, $\lambda_2/\lambda_1 = R(t_2)/R(t_1)$. If we let t_1 be arbitrary and t_2 the present time t_0, we have $\lambda_0/\lambda = R_0/R(t)$. This shift in wavelength is called redshift, and is defined to be $z \equiv \Delta\lambda/\lambda$. With $\Delta\lambda = \lambda_0 - \lambda$, we then have $1+z = R_0/R(t)$. If we differentiate this we get

$$\frac{{\rm d}z}{{\rm d}R} = \frac{\rm d}{{\rm d}R}\left(\frac{R_0}{R}\right) = -\frac{R_0}{R^2}. \tag{B.9}$$

Combing the former equation with $H = \dot{R}/R = ({\rm d}R/{\rm d}t)R \Rightarrow {\rm d}R/R = H{\rm d}t$ gives

$${\rm d}t = \frac{{\rm d}z}{H(z)(1+z)}. \tag{B.10}$$

To find $H(z)$ we go back to the Friedmann equation (B.4) and eq. (B.7). Let $\Omega_{\rm tot} = \Omega_{\rm m} + \Omega_{\rm r} + \Omega_{\rm v}$, then

$$\frac{k}{R_0^2} = H_0^2(\Omega_{\rm tot} - 1). \tag{B.11}$$

Remembering that $1 + z = R_0/R(t)$, we can rewrite the former equation for arbitrary times

$$\frac{k}{R^2} = \frac{k}{R_0^2}(1+z)^2 = H_0^2(\Omega_{\rm tot} - 1)(1+z)^2 \tag{B.12}$$

We then need to know how the different energy densities vary over time. For an adiabatic expansion, conservation of energy is ${\rm d}U = -P{\rm d}V$. With $P = w\rho$ and $U = \rho V \propto \rho R^3$, we have

$${\rm d}\left(\rho R^3\right) = -P{\rm d}\left(R^3\right) \tag{B.13}$$

$$\frac{{\rm d}\rho}{{\rm d}R}R^3 + 3\rho R^2 = -3w\rho R^2. \tag{B.14}$$

Separating variables and integrating gives

$$\rho \propto R^{-3(1+w)} = \left(\frac{1+z}{R_0}\right)^{3(1+w)}, \tag{B.15}$$

with $w = 0$ for matter and $w = 1/3$ for radiation. With this in mind, we divide the Friedmann equation (B.4) by $H_0^2 = (8\pi/3)G\rho_{\text{crit}}$ and obtain

$$\begin{aligned}\frac{H(z)^2}{H_0^2} &= (1 - \Omega_{\text{tot}})(1+z)^2 + \Omega_{\text{v}}(1+z)^{3+3w} \\ &\quad + \Omega_{\text{m}}(1+z)^3 + \Omega_{\text{r}}(1+z)^4.\end{aligned} \tag{B.16}$$

The density contribution from relativistic particles are very small, so we can neglect Ω_{r}. The vacuum energy (dark energy) acts like a cosmological constant with $w = -1$. With $\Omega_{\text{tot}} \approx 1$ eq. (B.16) is then simplified to

$$H(z) = H_0[\Omega_{\text{v}} + \Omega_{\text{m}}(1+z)^3]^{1/2}. \tag{B.17}$$

Today's values are estimated to be $H_0 = (72.0 \pm 3.0)\,\text{km}\,\text{s}^{-1}\,\text{Mpc}^{-1}$, $\Omega_{\text{v}} = 0.68 \pm 0.02$, and $\Omega_{\text{m}} = 0.32 \pm 0.01$ assuming $k = 0$ [35].

Bibliography

[1] ESA. The Hipparcos Space Astrometry Mission: Hertzsprung-Russell Diagrams, 2007.

[2] Swinburne Astronomy Online. Cosmos - the SAO Encyclopedia of Astronomy: Type Ib Supernova Spectra, 2014.

[3] J.K. Truelove and C.F. McKee. Evolution of nonradiative supernova remnants. *ApJS*, 120:299–326, 1999. (doi:10.1086/313176).

[4] D.J. Whalen et al. Pair-instability supernovae in the local universe. *ApJ*, 797:9, 2014. (arXiv:1312.5360v2 [astro-ph.HE]).

[5] D.J. Whalen et al. Finding the first explosions I: pair-instability supernovae. *ApJ*, 777:110, 2013. (arXiv:1211.4979v4 [astro-ph.CO]).

[6] J. Smidt et al. Finding the first explosions. IV. 90-140 $M_{\odot}$ pair-instability supernovae. arXiv:1411.5377v1 [astro-ph.HE], 2014.

[7] V.A. Dogiel V.L. Ginzburg V.S. Berezinsky, S.V. Bulanov and V.S. Ptuskin. *Astrophysics of Cosmic Rays*. North-Holland, 1990.

[8] D. Prialnik. *An Introduction to the Theory of Stellar Structure and Evolution*. Cambridge University Press, 2nd edition, 2010.

[9] M.L. Kutner. *Astronomy - a Physical Perspective*. Cambridge University Press, 2nd edition, 2003.

[10] C. Raskin et al. Remnants of binary white dwarf mergers. *ApJ*, 746:62, 2012. (arXiv:1112.1420 [astro-ph.HE]).

[11] M. Turatto. Classification of supernovae. arXiv:astro-ph/0301107, 2003.

[12] E. Chatzopoulos and J.C. Wheeler. Effects of rotation on the minimum mass of primordial progenitors of pair-instability supernovae. *ApJ*, 748:42, 2012. (arXiv:1201.1328 [astro-ph.HE]).

[13] D.J. Whalen et al. Finding the first explosions. III. pulsational pair-instability fupernovae. *ApJ*, 781:106, 2014. (arXiv:1311.1221v3 [astro-ph.CO]).

[14] R.S. de Souza et al. Probing the stellar initial mass function with high-z supernovae. *MNRAS*, 442:1640–1655, 2014. (arXiv:1401.2995 [astro-ph.CO]).

[15] A. Loeb T. Pan and D. Kasen. Pair-instability supernovae via collision runaway in young dense star clusters. *MNRAS*, 423:2203–2208, 2012. (arXiv:1111.3648 [astro-ph.HE]).

[16] D.R. Young et al. Two type ic supernovae in low-metallicity, dwarf galaxies: Diversity of explosions. *A&A*, 512:A70, 2010. (arXiv:0910.2248 [astro-ph.CO]).

[17] A. Gal-Yam et al. Supernova 2007bi as a pair-instability explosion. *Nature*, 462:624, 2009. (arXiv:1001.1156 [astro-ph.CO]).

[18] J. Cooke et al. Super-luminous supernovae at redshifts of 2.05 and 3.90. *Nature*, 419:228, 2012. (arXiv:1211.2003 [astro-ph.CO]).

[19] M.J. Thompson. *An Introduction to Astrophysical Fluid Dynamics*. Imperial College Press, 2006.

[20] J.I. Katz. *High Energy Astrophysics*. Addison-Wesley Publishing Company, Inc., 1987.

[21] C.F. McKee D.F. Cioffi and E. Bertschinger. Dymamics of radiative supernova remnants. *ApJ*, 334:252–265, 1988. (doi:10.1086/166834).

[22] T.K. Gaisser. *Cosmic Rays and Particle Physics*. Cambridge University Press, 1990.

[23] A.R. Bell. The acceleration of cosmic rays in shock fronts - I. *MNRAS*, 182:147–156, 1978.

[24] A.R. Bell. Non-linear amplification of a magnetic field driven by cosmic ray streaming. *MNRAS*, 353:550–558, 2004. (doi:10.1111/j.1365-2966.2004.08097.x).

[25] L.O'C. Drury. An introduction to the theory of diffusive shock acceleration of energetic particles in tenuous plasmas. *Rep. Prog. Phys.*, 46:973–1027, 1983. (doi:10.1088/0034-4885/46/8/002).

[26] M.S. Longair. *High Energy Astrophysics*. Cambridge University Press, 3rd edition, 2011.

[27] M. Ahlers K. Murase and B.C. Lacki. Testing the hadronuclear origin of PeV neutrinos observed with IceCube. *Phys.Rev.D*, 88:121301(R), 2013. (arXiv:1306.3417 [astro-ph.HE]).

[28] M. Kachelriess. Lecture notes on high energy cosmic rays, 2007. arXiv:0801.4376 [astro-ph].

[29] E.E. Salpeter. The luminosity function and stellar evolution. *ApJ*, 121:161–167, 1955. (doi:10.1086/145971).

[30] R.S. de Souza et al. Detectability of the first cosmic explosions. *MNRAS*, 436:1555âĂŞ1563, 2013. (arXiv:1306.4984 [astro-ph.CO]).

[31] B.C. Lacki. OlberâĂŹs paradox for superluminal neutrinos: Constraining extreme neutrino speeds at TeV-ZeV energies with the diffuse neutrino background. *JCAP*, 01:,54, 2012. (arXiv:1111.3045v2 [hep-ph]).

[32] A.W. Strong et al. Turbulent amplification of magnetic field and diffusive shock acceleration of cosmic rays. *ApJ*, 722:L58, 2010. (arXiv:1008.4330v1 [astro-ph.HE]).

[33] G.B. Rybicki and A.P. Lightman. *Radiative Processes in Astrophysics*. Wiley-VCH, 2004.

[34] M. Kachelriess. Lecture notes for FY3452 Gravitation and Cosmology, 2013.

[35] K.A. Olive et al. (Particle Data Group). Review of particle physics. *Chin. Phys. C*, 38:090001, 2014. doi:10.1088/1674-1137/38/9/090001.